II. Primary Hydrogen Burning Phases

II.1 The Main Sequence

Figure 10 shows the hydrogen burning evolution from the ZAMS to the red-giant branch (hereafter RGB) for various masses. Table 2 lists times taken to traverse between the given points. For hydrogen burning we have H $\rightarrow$ He, so as the hydrogen mass fraction decreases the mean molecular weight μ increases. But

$$P = \frac{\rho \Re T}{\mu}.$$

So hydrogen burning causes the pressure to decrease. But if this happens then the star contracts, increasing the temperature and density. The nett effect is for the pressure to remain roughly constant, at a value large enough to support the outer layers, while the central density and temperature increase. But if the temperature increases then the energy generation increases since

$$\epsilon \sim \rho X^2 T^n,$$

so that the overall luminosity also increases. This energy is partly absorbed in the surrounding envelope. This is especialy true for stars with radiative envelopes (on the upper main sequence), so that the absobed energy does work against the gravitational field, and the radius increases. Then since

$$L = 4\pi R^2 \sigma T_e^4$$

the effective temperature decreases. The star moves up and to the right in the HR diagram. For lower main sequence stars, with convective enveopes, we may expect that the very efficient energy transport in the convective envelope will transport all the liberated energy to the surface, with little absorption. Thus the radius is, to first order, constant, and the overall effective temperature increases due to the increase in L.

So hydrogen burning on the main sequence is accompanied by rising luminosity and either decreasing T_e (upper main sequence, higher masses) or increasing T_e (lower main sequence, lower masses). This is indeed seen in figure 10. Note the dashed lines, which indicate the main sequence band containing stars burning hydrogen in their cores. The lower dashed line is the ZAMS.

To understand the interior structure see Figure 11 which shows the variation of many variables with mass fraction for a $1M_\odot$ star on the main sequence, between points 1 and 2 in figure 10. Note the radiative core (leading to a smooth variation of X with mass). Figure 12 shows the same star just after core hydrogen exhaustion, and we see the dense, isothermal hydrogen-exhausted core is developing.

Figure 13 shows the hydrogen profiles (*i.e.* X versus $M(r)$) for a $1M_\odot$ star at different times. The smooth variation is quite different from the result when a convective core is present. In this case the rapid convective timescale means that the composition is homogenized in the convective region on a very short time-scale. Hence we get hydrogen profiles like those shown in figure 14, where we see that the mass of the convective core has *decreased* with time (in the figure $t_0 < t_1 < t_2$).

We have mentioned how convection is an uncertainty in stellar evolution. Recall the mixing length theory, discussed earlier. Here we found that the convective velocity v was given by

$$v \propto (\nabla - \nabla_{ad})^{1/2}.$$

This was derived assuming buoyancy (*i.e.* acceleration) due to $D\rho$. So at the edge of the convective core, where $\nabla = \nabla_{ad}$, we have zero buoyancy, so there is zero acceleration. But an

element which began its motion inside the convective core still has momentum at the boundary. True, the acceleration is zero at the boundary, and negative in the outer radiative zone, but the acceleration is positive everywhere in the convective zone. So the element reaches the boundary with a finite velocity. The element then continues its motion into the radiatively stable zone. This phenomenon is called "convective overshoot" and results in the mixing of part of the radiatively stable zone with the convective zone. It thus effectively extends the convective boundary beyond that determined by the Schwarzschild or Ledoux criteria.

One way of including this effect is to calculate the restoring force on the element as it moves through the stable region. Thus we can calculate where it comes to rest, and mix the material out to this point. The result of such a calcuation is shown in figure 15. Note that $v = 0$ some $0.043\ M$ beyond the Schwarzschild boundary (where $\nabla = \nabla_{ad}$).

How does this affect the evolution ? Clearly it makes the convective core larger. Hence more hydrogen fuel is mixed to the centre. We may expect hydrogen burning to last longer, and indeed it does. The efficiency of overshooting is dependent on the miximg-length parameter α:

$$\alpha = \frac{\ell_{mix}}{H_P}.$$

Obviously $\alpha = 0$ corresponds to no overshooting. Figure 16 shows the change in hydrogen profiles (at hydrogen exhaustion) with α, and the corresponding HR diagram paths for a star of $M = 7M_\odot$.

II.2 Core Hydrogen Exhaustion and the Giant Branch

In low mass stars hydrogen is exhausted initially in a tiny region, which grows with time. With a temperature gradient existing the only was the star can provide energy is by contracting. This it does slowly, so that the hydrogen rich layers are gradually brought to higher T and ρ, and begin burning. A shell source is ignited, and the star evolves to the right in the HR diagram. Conditions in a $1M_\odot$ star at this time are shown in figure 17.

For higher masses the evolution is similar. But if a convective core exists the sudden depletion of fuel over a larger region causes a more rapid contraction over this inner region. This gives the kink between points 2 and 3 seen in figure 10 for the more massive stars.

The evolution to the right occurs at nearly constant luminosity, and is very rapid (see Table 2). For this reasone very few stars are seen in this phase, and this region of the HR diagram is called the "Hertzsprung Gap", or the "sub-giant branch". This phase is accompanied by a large radius increase, hence T_e decreases since

$$L \sim R^2 T_e^4.$$

i.e. the star becomes a red giant. For cool envelope temperatures the opacity increases, and convection develops. The "giant branch" is the nearly vertical line corresponding to a fully convective star, also known as the Hayashi track.

Convection actually extends sufficiently far inward to reach places where partial hydrogen burning has occurred, with C and O being processed into N, and some H into He. Thus this H-processed material is mixed to the surface. This is called the "first dredge-up" episode, and we actually observe the increased N^{14} abundance on the giant branch, as predicted.

All stars now ascend the giant branch, with the hydrogen exhausted core contracting slowly, and thus heating. The hydrogen burning shell is eating its way outward (in mass) through the hydrogen rich envelope, and leaving behind He "ashes" which become part of the growing helium core. Eventually this core becomes hot enough for He ignition. For low mass stars the core wil be degenerate at this time, and a core helium flash will occur. For more massive stars the He is ignited gently.

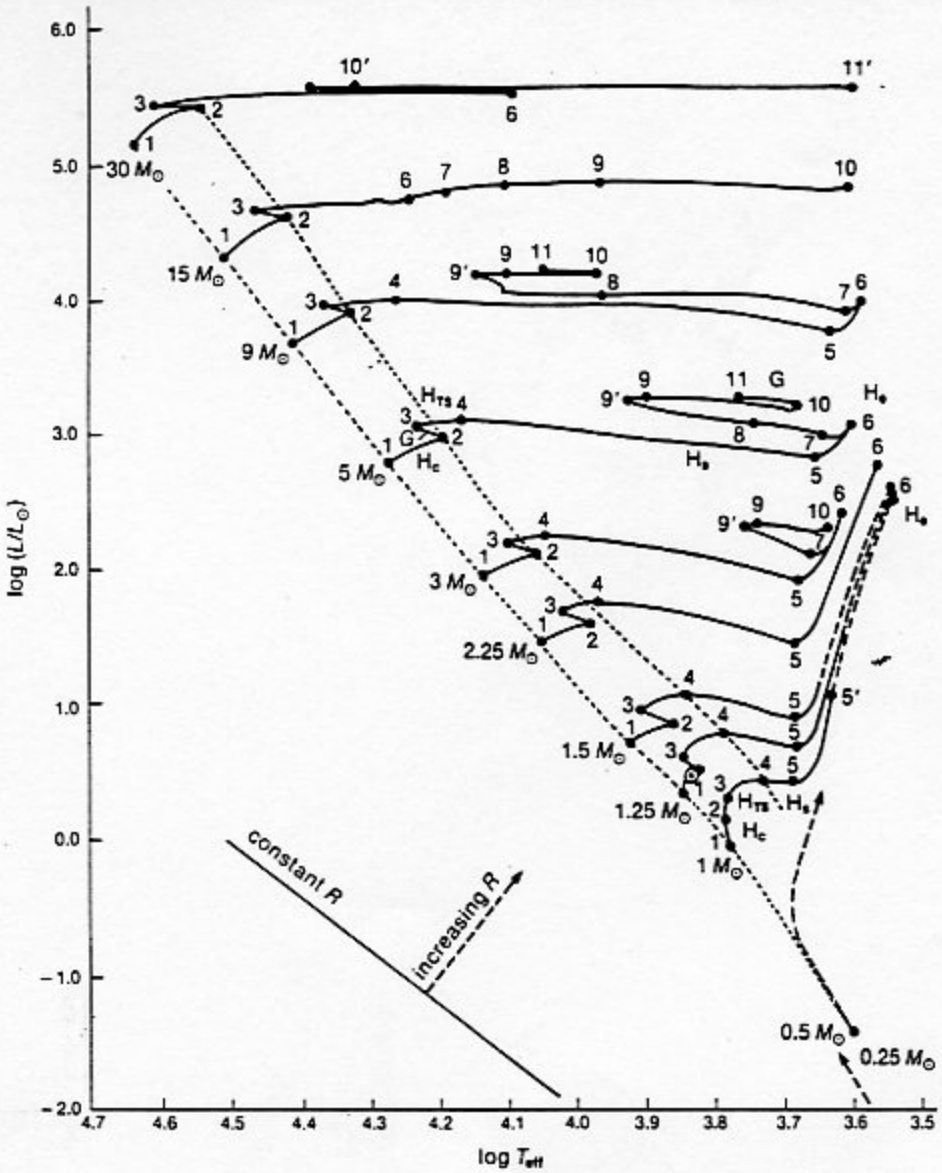

Fig 10

Figure 9.1. Evolutionary tracks for models of stars after the main sequence. Model mass is shown next to the initial point on zero age main sequence. Dotted lines indicate boundaries of the main sequence. Lines of constant radius and increasing radius as shown in lower left. Elapse times between points are shown in Table 9.1. The stages are labeled as: H_c, hydrogen core burning; H_{TS}, thick hydrogen shell burning; H_s, shell hydrogen burning; He, helium core burning; and G, gravitational energy release. The 15 $M_\odot$ track does not reverse in the giant region, because the semiconvective region was treated as fully convective in this model.

Table 2

Table 9.1
Elapsed time, in years, between numbered points on the evolutionary tracks in Figure 9.1. Numbers in parentheses are powers of 10 by which entries are multiplied.

	Interval				
Mass ($M_\odot$)	1–2	2–3	3–4	4–5	5–6
30	4.80 (6)	8.64 (4)	←	−1.0 (4) →	
15	1.010 (7)	2.270 (5)	←	7.55 (4) →	
9	2.144 (7)	6.053 (5)	9.113 (4)	1.477 (5)	6.552 (4)
5	6.547 (7)	2.173 (6)	1.372 (6)	7.532 (5)	4.857 (5)
3	2.212 (8)	1.042 (7)	1.033 (7)	4.505 (6)	4.238 (6)
2.25	4.802 (8)	1.647 (7)	3.696 (7)	1.310 (7)	3.829 (7)
1.5	1.553 (9)	8.10 (7)	3.490 (8)	1.049 (8)	≥2 (8)
1.25	2.803 (9)	1.824 (8)	1.045 (9)	1.463 (8)	≥4 (8)
1.0	7 (9)	2 (9)	1.20 (9)	1.57 (8)	≥1 (9)

	Interval				
Mass ($M_\odot$)	6–7	7–8	8–9	9–10[a]	10[a]–11[a]
30		53.1 (4)			1.3 (4)
15	7.17 (5)	6.20 (5)	1.9 (5)	3.5 (4)	
9	4.90 (5)	9.50 (4)	3.28 (6)	1.55 (5)	2.86 (4)
5	6.05 (6)	1.02 (6)	9.00 (6)	9.30 (5)	7.69 (4)
3	2.51 (7)	4.08 (7)		6.00 (6)	

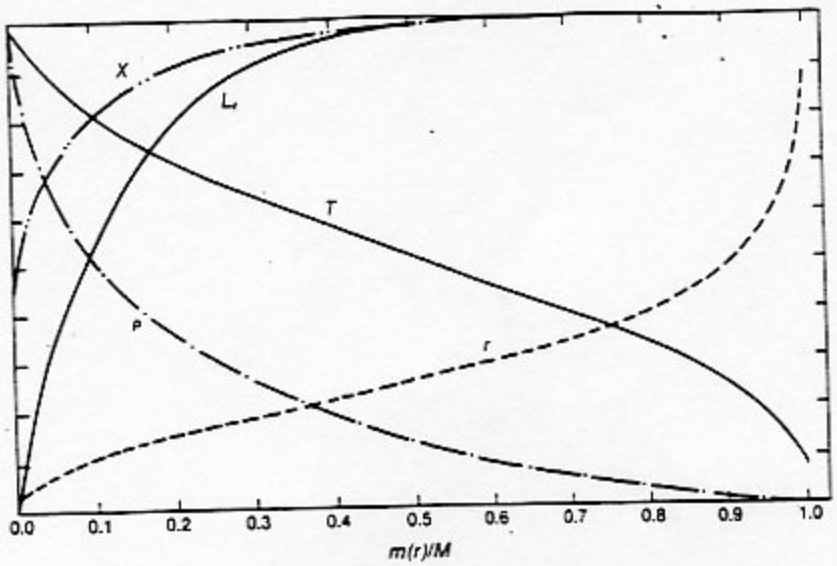

Fig 11

Figure 9.2. A 1 $M_\odot$ model during main-sequence hydrogen burning at time 4.2699×10^9 years (between points 1 and 2 in Figure 9.1), showing radius, density, temperature, total luminosity, and hydrogen abundance versus mass fraction. The lower limits of the ordinate are zero. The upper limit for each curve is: $r = 0.9683\ R_\odot$, $\rho_c = 159.93\ \text{g cm}^{-3}$, $T_c = 1.591 \times 10^7$ K, $L = 1.0575\ L_\odot$, and $X_c = 0.708$; $P_c = 2.5186 \times 10^{17}$ dynes cm^{-2}. The elapsed time is measured from the initial model for the phase before the main sequence.

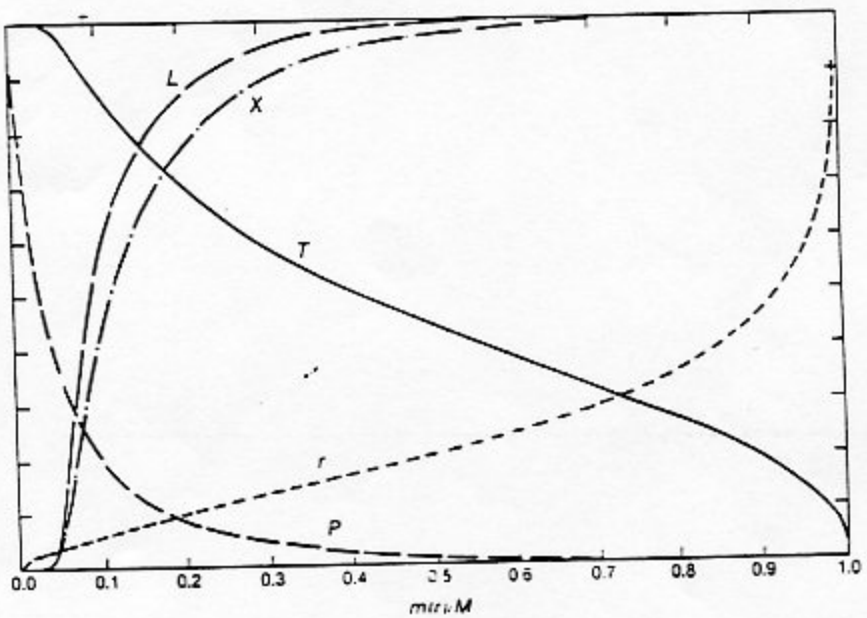

Fig 12

Figure 9.3. Same as Figure 9.2 for 1 $M_\odot$ model between points 2 and 3 of Figure 9.1. The elapsed time since the initial model for the phase before the main sequence is 9.2015×10^9 years. The lower limits of the ordinate are zero. The upper limit of the ordinate for each curve is $r = 1.268\ R_\odot$; $P_c = 1.315 \times 10^{18}$ dynes cm^{-2}; $T_c = 1.91 \times 10^7$ K; $L = 2.13\ L_\odot$; $X_c = 0.708$. The actual stellar radius is $R = 1.353\ R_\odot$, and the central density is 1026.0 g cm^{-3}.

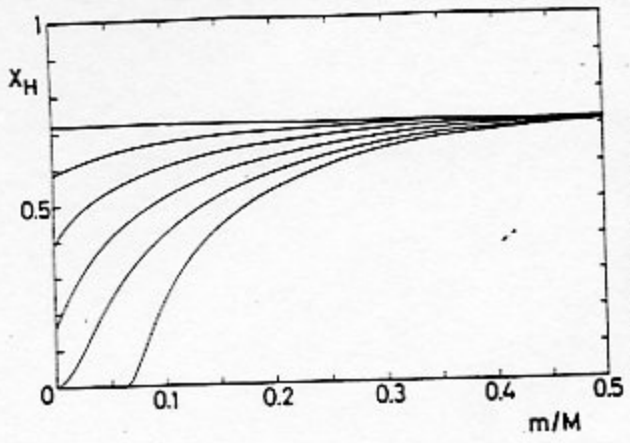

Fig. 30.1. Hydrogen profiles showing the gradual exhaustion of hydrogen in a star of $1M_\odot$. The homogeneous initial model consists of a mixture with $X_H = 0.723$. The hydrogen content X_H over m/M is plotted for six models which correspond to an age of 0.0, 2.2, 4.5, 6.7, 8.9 and 11.4 times 10^9 years after the onset of hydrogen burning

13

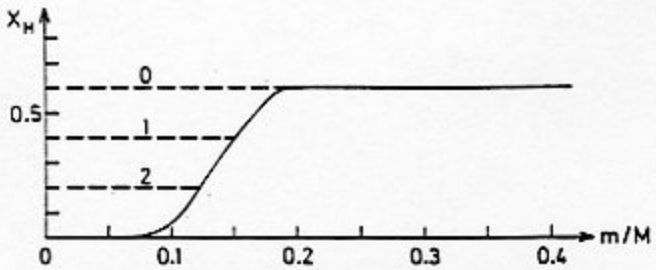

Fig. 30.2. The solid line gives the hydrogen profile $X_H(m)$ that is established in a $5M_\odot$ star of extreme population I at the end of hydrogen burning in a shrinking convective core. The dashed lines indicate the hydrogen content in the convective core at the onset (label 0) and at two intermediate phases of central hydrogen burning

14

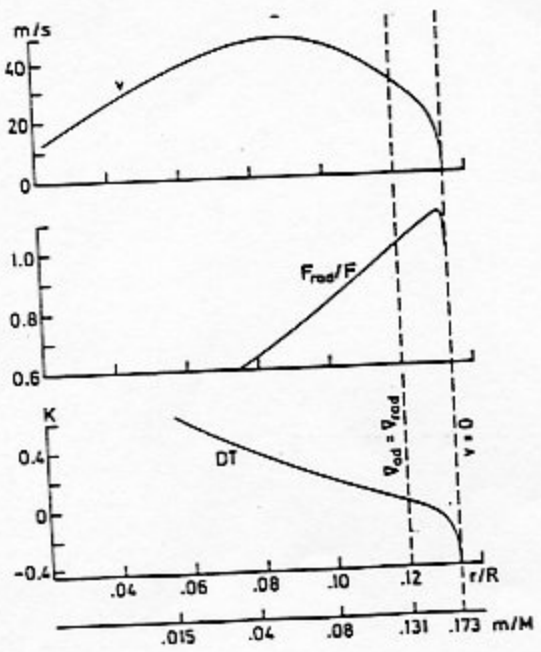

Fig. 30.4. Velocity v and temperature excess DT of rising convective elements, and the ratio of the radiation flux F_{rad} relative to the total flux F around the border of stability ($\nabla_{rad} = \nabla_{ad}$) in a star of $2M_\odot$. Overshooting calculated with $\alpha = l_m/H_P = 1$ extends to the point where $v = 0$ (after MAEDER, 1975)

15

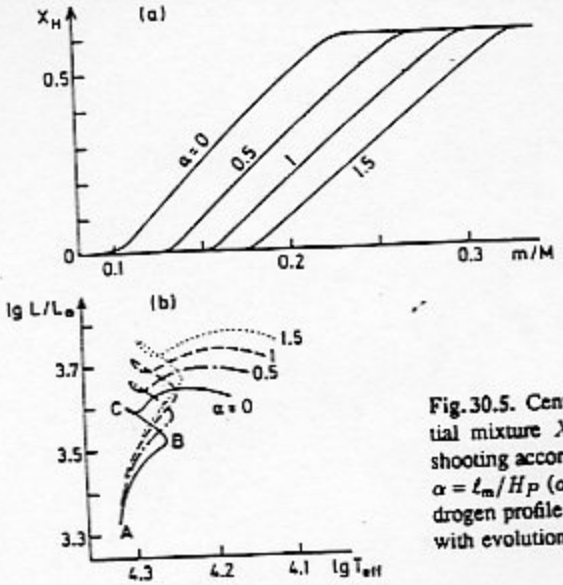

16

Fig. 30.5. Central hydrogen burning for a $7\,M_\odot$ star (initial mixture $X_H = 0.602$, $X_{He} = 0.044$) with overshooting according to different assumptions for the ratio $\alpha = \ell_m / H_P$ ($\alpha = 0$ means no overshooting). (a) The hydrogen profile at the end of this phase. (b) HR diagram with evolutionary tracks. (MATRAKA et al., 1982)

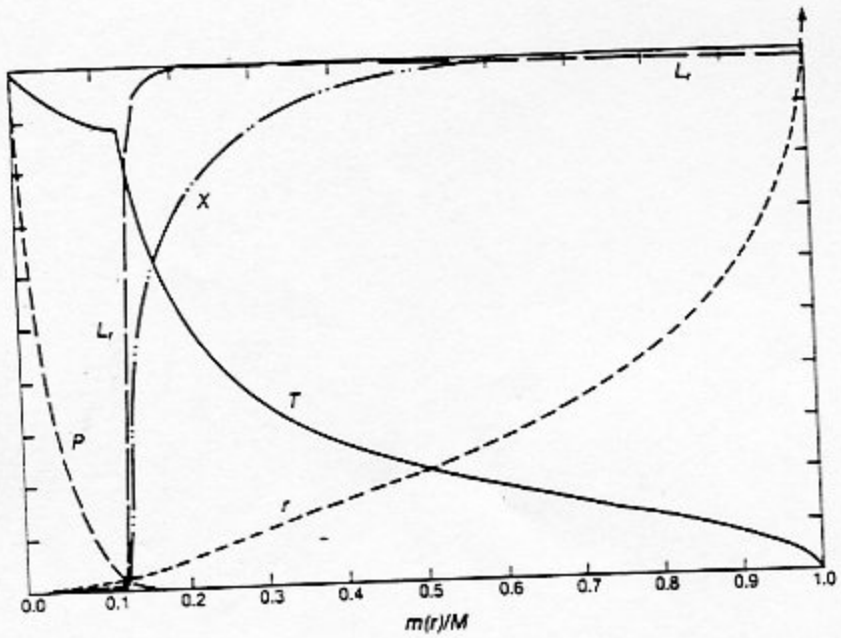

17

Figure 10.7. Model of a 1 $M_\odot$ star just after it leaves the main sequence, at time 10.31×10^9 years. The maximum value of the ordinate for each curve is: $r = 2.13\ R_\odot$; $P_c = 5.15 \times 10^{15}$ dynes cm^{-2}; $T_c = 2.39 \times 10^7$ K; $L = 2.82\ L_\odot$; $X = 0.708$. The total radius is 2.2179 $R_\odot$, and the central density is 1.52×10^4 g cm^{-3}. Note the gradual increase in L for $m(r)/M \geq 0.4$.

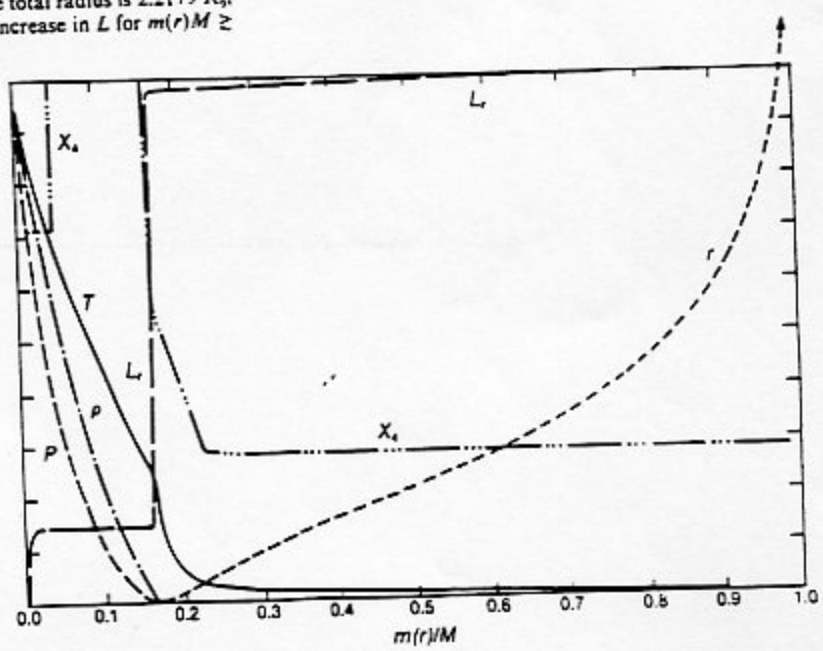

18

Figure 10.12. The 5 $M_\odot$ during the giant stage at time 7.7×10^7 years. The maximum values of the ordinate for each curve are: $r = 35.85\ R_\odot$; $P_c = 6.21 \times 10^{15}$ dynes cm^{-2}; $\rho_c = 7.7$ g cm^{-3}; $T_c = 1.33 \times 10^8$ K; $L = 1.14\ L_\odot$; and helium abundance $X_4 = 0.9763$. Total radius $R = 50.61\ R_\odot$.

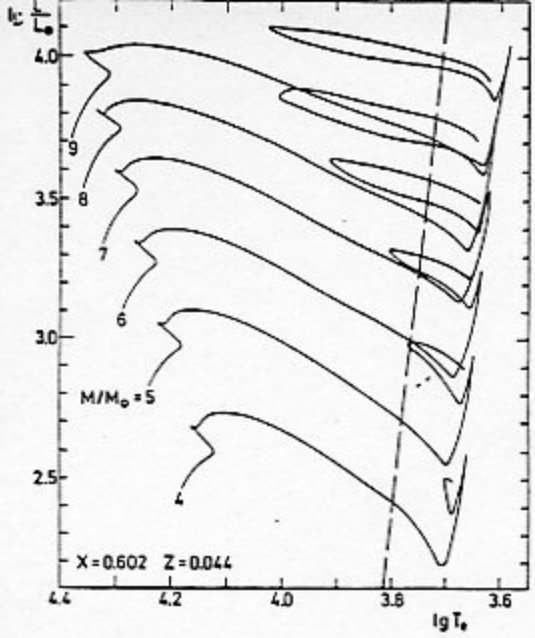

Fig. 31.6. Hertzsprung–Russell diagram with evolutionary tracks for stars in the mass range from $4M_\odot$ to $9M_\odot$ from the main sequence through helium burning (after MATRAKA et al., 1982). The broken line indicates the Cepheid strip

19

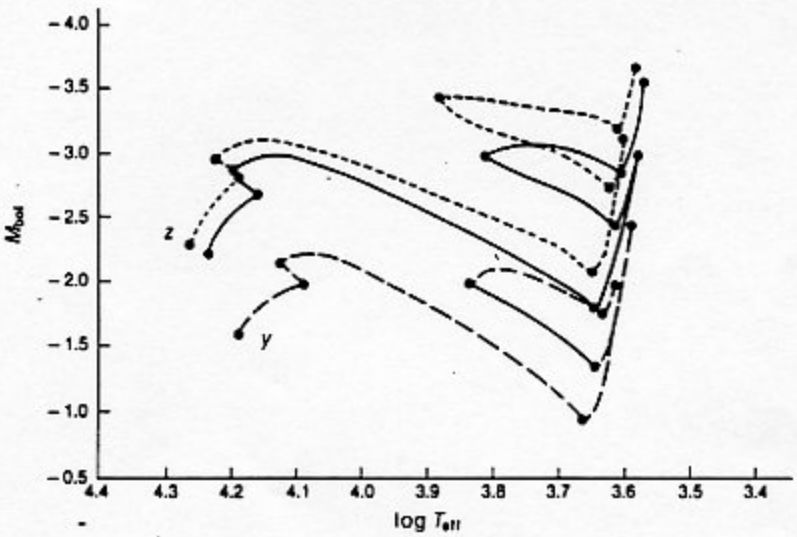

20

Figure 10.16. Effect of chemical composition on the evolutionary track for a Population I star of mass 5 $M_\odot$. The compositions are: solid curve, $X = 0.67$, $Y = 0.30$, and $Z = 0.03$; (dashed curve, $Y = 0.20$ and $Z = 0.03$; dotted curve, $Y = 0.30$ and $Z = 0.015$).

21

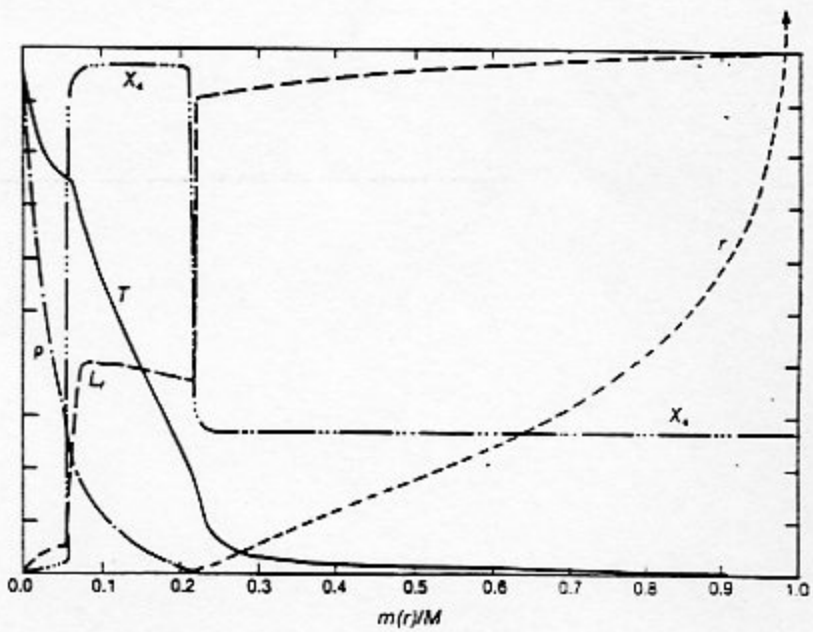

Figure 10.13. Model of a 5 $M_\odot$ star during the giant stage at time 8.79×10^7 years. Maximum ordinate for each curve: $r = 23.77\ R_\odot$ (total radius $R = 44.14\ R_\odot$); $\rho_r = 2.16 \times 10^4$ g cm^{-3}; $T_r = 1.84 \times 10^8$ K; $L = 1.94\ L_\odot$; and $X_c = 1.0$.

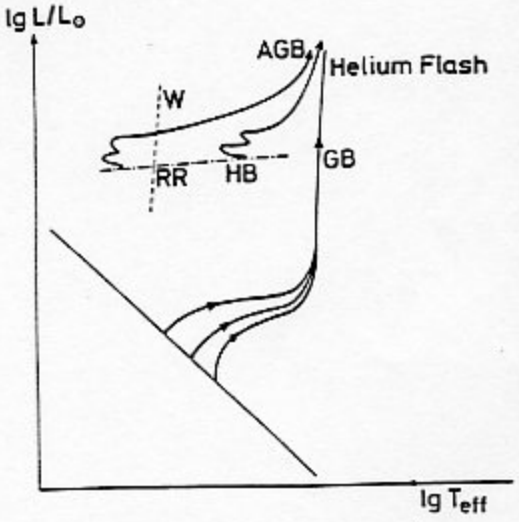

Fig. 32.10. Sketch of the evolution of low-mass stars in the HR diagram. For three slightly different masses the evolutionary tracks in the post-main-sequence merge in the giant branch (GB). After the helium flash they appear on the zero-age horizontal branch (HB), evolve towards the upper right, and merge in the asymptotic giant branch (AGB). The broken line indicates the positions of the variable RR Lyr stars (RR) and of the W Vir stars (W)

22

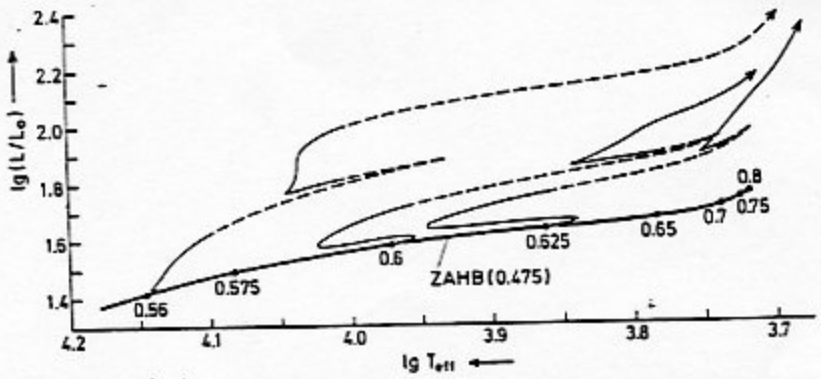

Fig. 32.9. Hertzsprung–Russell diagram with the zero-age horizontal branch and the evolution afterwards. The thick line labelled with ZAHB is the zero-age horizontal branch for models with a helium core of $M_c = 0.475 M_\odot$ and a hydrogen-rich envelope ($X_H = 0.699$, $X_{He} = 0.3$) with different masses $M - M_c$. The total masses M (in $M_\odot$) are indicated for a few points. For 3 of these models the ensuing evolution is shown by the thin lines. Phases of slow evolution are given by solid lines, those of rapid evolution by broken lines. The models evolve from the ZAHB first in the slow phase of central helium burning with a hydrogen-burning shell. This phase, which lasts for some 10^7 years, is followed by a phase of rapid evolution during which the models go from helium burning in the centre to shell burning. After that a slow phase of double shell burning occurs. (After STROM et al., 1970. See also IBEN, ROOD, 1970)

23

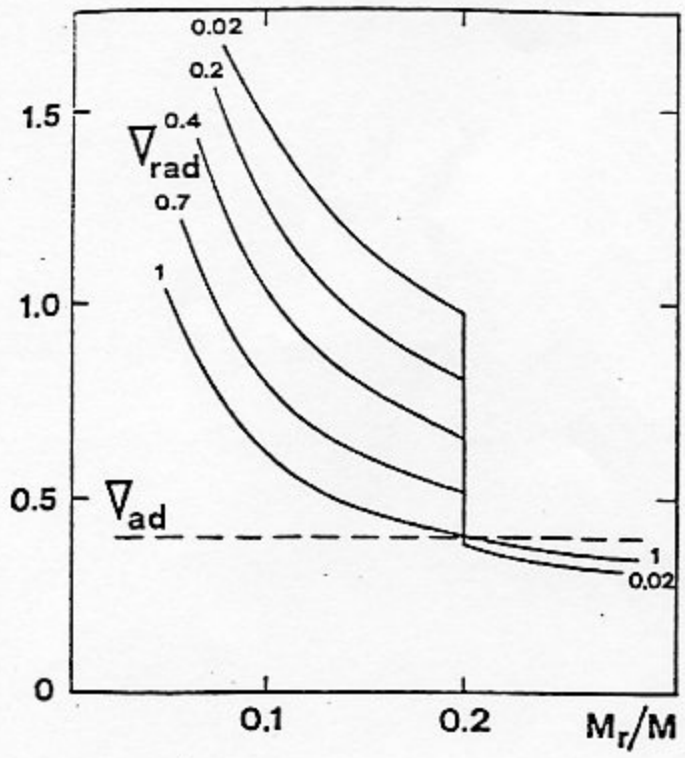
0.02
0.2
0.4
0.7
1
∇_{rad}
∇_{ad}
1.5
1.0
0.5
0
0.1
0.2
M_r/M
1
0.02

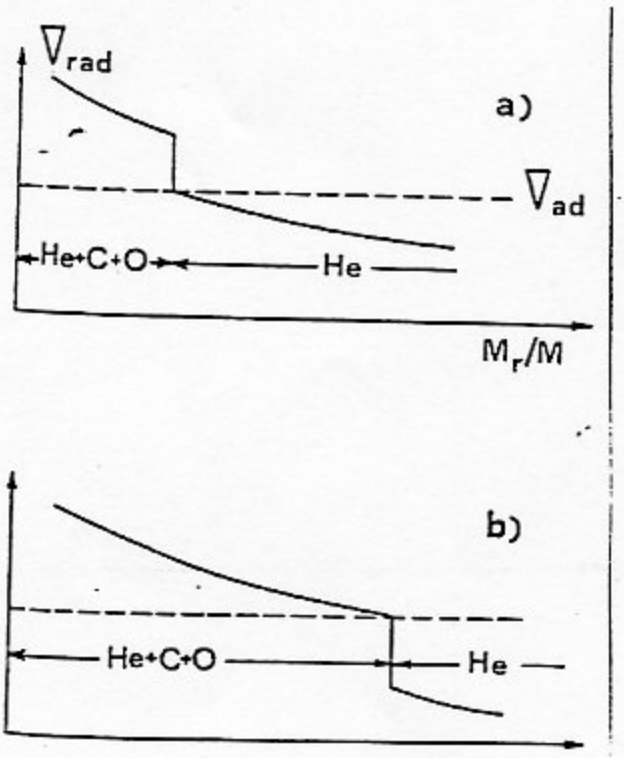
∇_{rad}
a)
∇_{ad}
He+C+O
He
M_r/M
b)
He+C+O
He

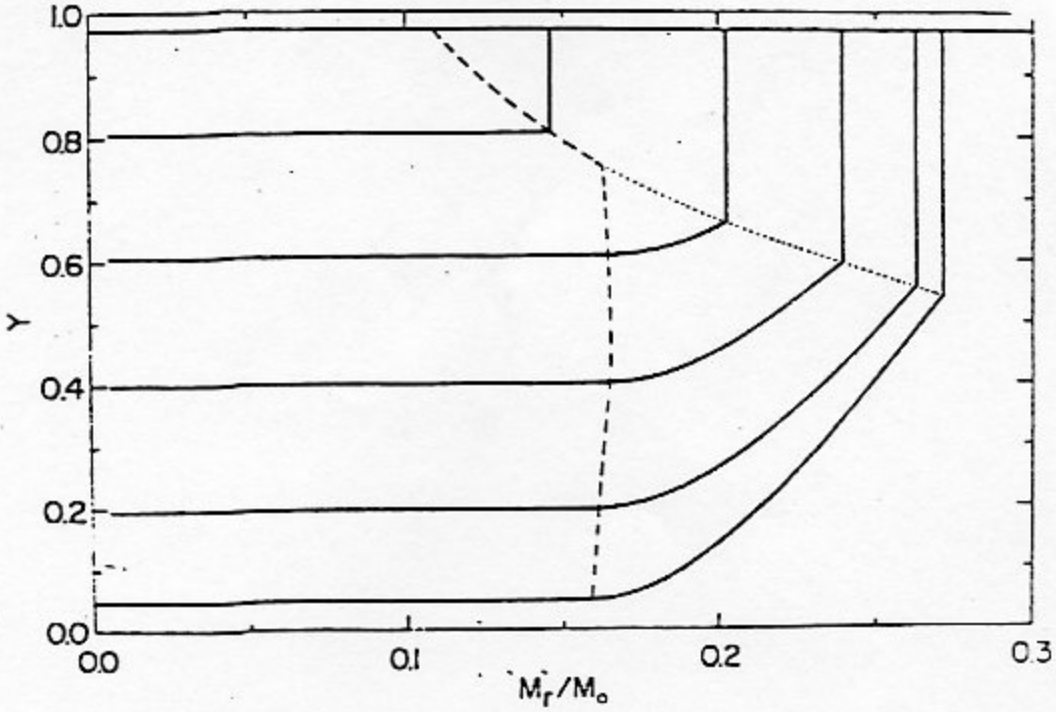

25

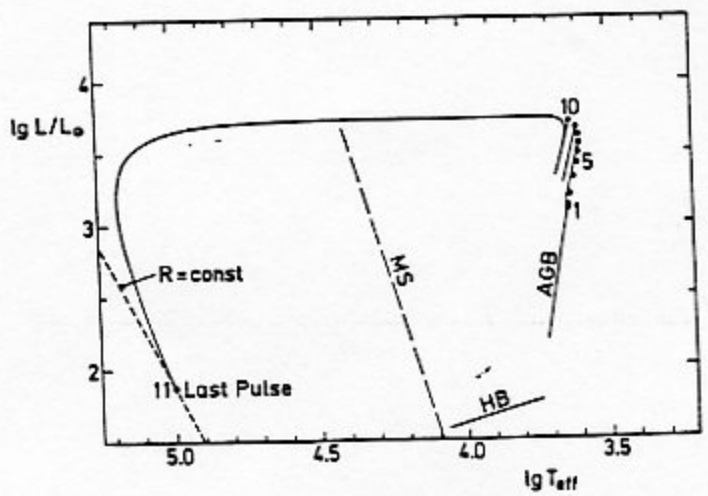

Fig. 32.11. The evolutionary track of a star of $0.6M_\odot$ ($X_H = 0.749$, $X_{He} = 0.25$) for the phases after central helium burning. The model moves upwards along the asymptotic giant branch (AGB) until thermal pulses occur (indicated by full circles). The changes during a pulse are shown only for pulse 9 and pulse 10. Before the last pulse the track has reached the white-dwarf area of the HR diagram. The main sequence (MS), the horizontal branch (HB), and a line of constant radius in the white-dwarf region are indicated (after IBEN, RENZINI, 1983)

26

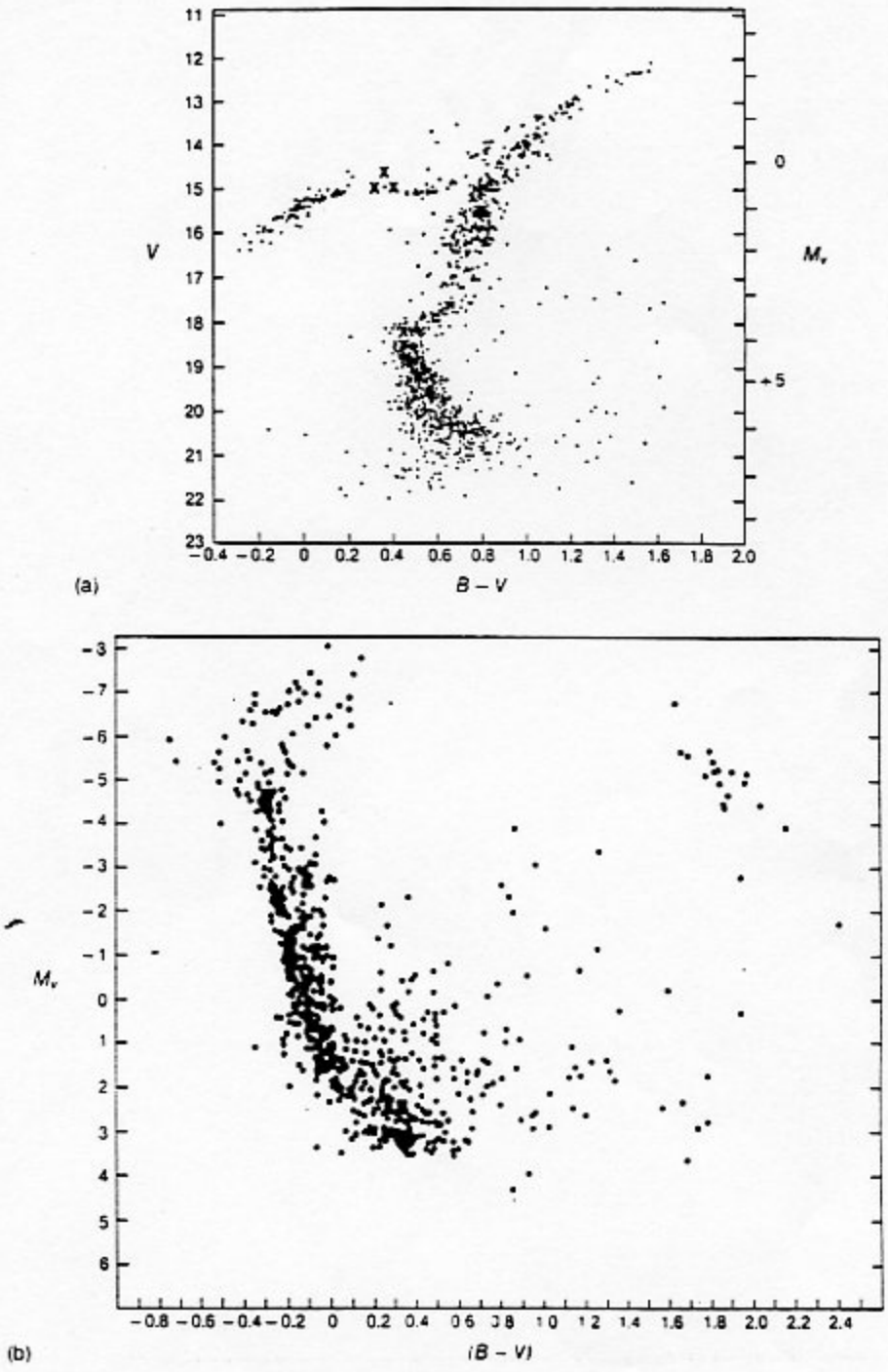

Figure 3.4. Color-magnitude diagram for: (a) a typical globular cluster, M5, in Serpens (Population II stars); and (b) a typical galactic cluster, h and χ Persei (Population I stars). $(B - V)_0$ is the observed color index. Positions of RR Lyrae variables are denoted by x.

27

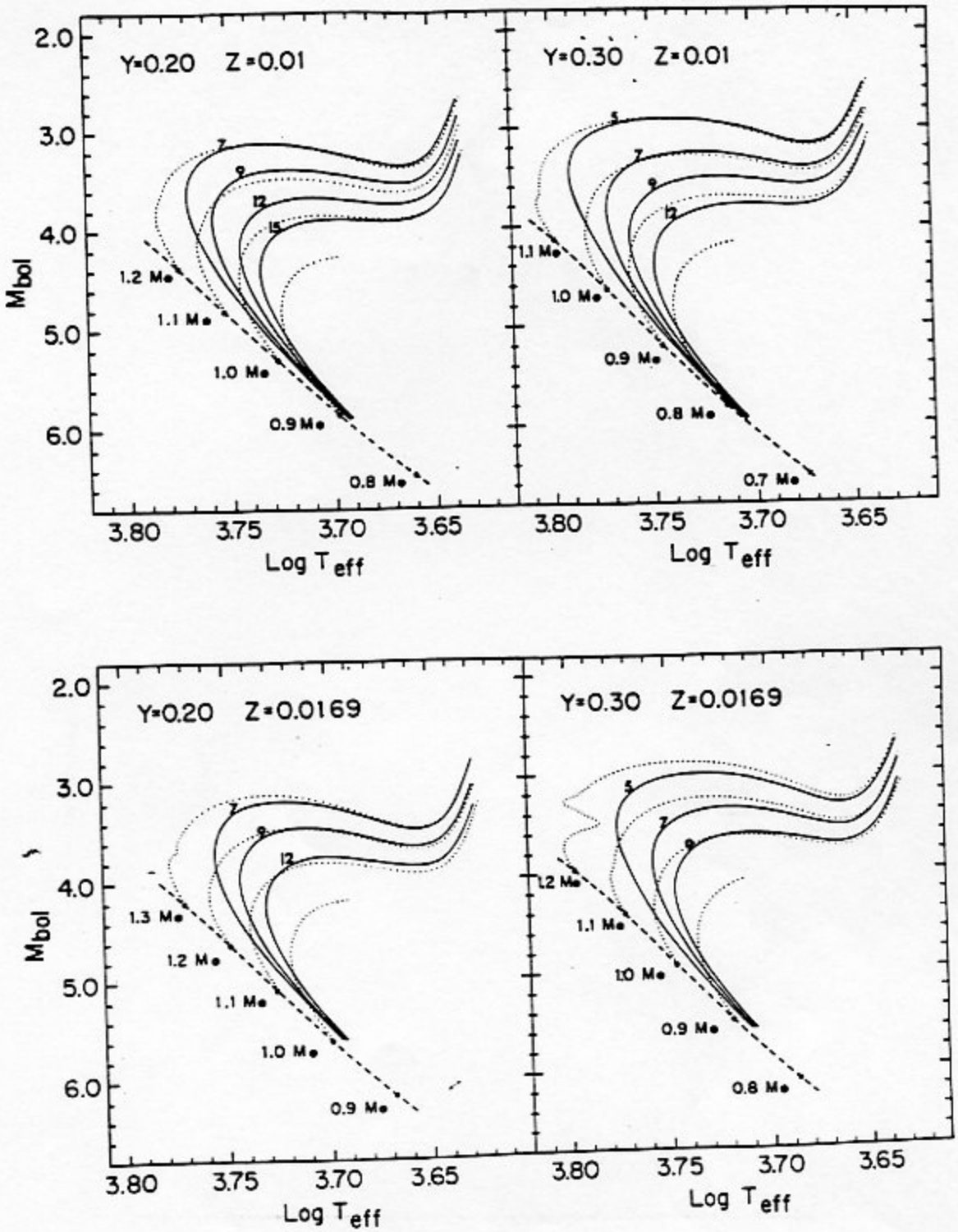

FIG. 2.—*Continued*

28

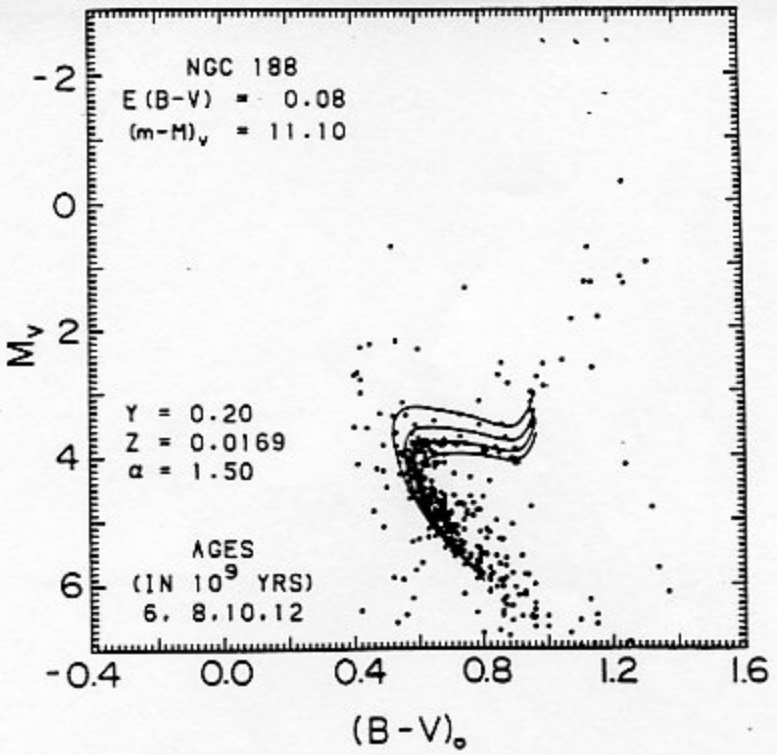

29

FIG. 10.—Similar to Fig. 7; in this case the data of NGC 188, which has [Fe/H] = 0.0, are fitted by the relevant set of theoretical isochrones.

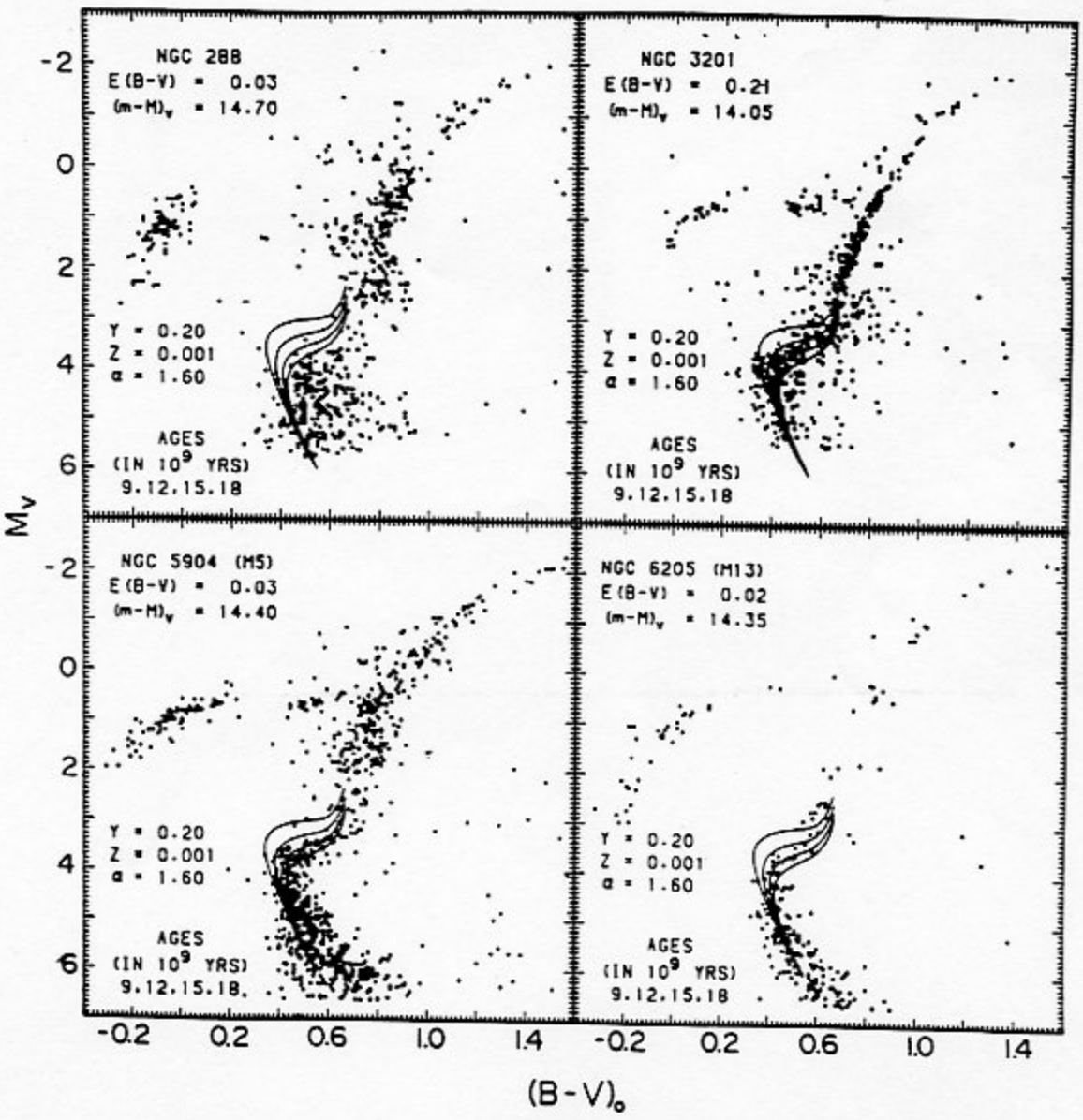

30

FIG. 8.—Similar to Fig. 7; in this case the data of NGC 288, NGC 3201, M5, and M13, which have [Fe/H] = −1.3, are fitted by the relevant set of theoretical isochrones.

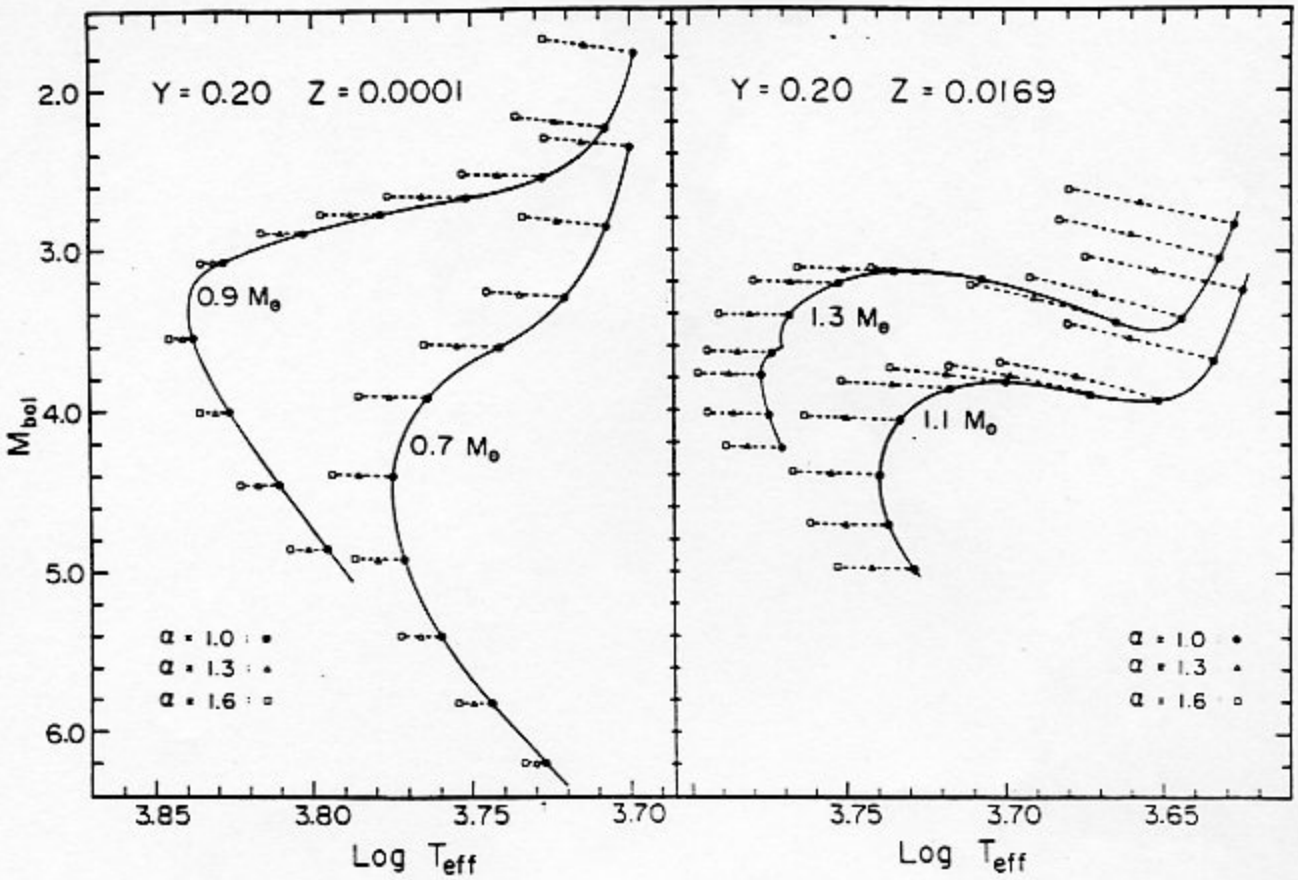

FIG. 3.—Location on the H-R diagram, as a function of the mixing-length parameter, of various models along two metal-poor and two metal-rich evolutionary sequences reproduced from Fig. 1. Filled circles, open triangles, and open squares give, respectively, the model positions for $\alpha = 1.0$, $\alpha = 1.3$, and $\alpha = 1.6$.

Table 3). If the model sequences obtained by connecting the squares in Figure 3 are compared with those, for the same masses and compositions, which are computed in their entirety for $\alpha = 1.6$, nearly perfect agreement is found, except that the level of the subgiant branch predicted by the former is too bright. This result applies only to the metal-rich calculations (the tracks for $Z = 10^{-4}$ were indistinguishable) where, for instance, δM_{bol} was ~ 0.06 mag at $\log T_{eff} = 3.71$ for the $1.1 M_{\odot}$ model. We conclude, hence, that our adopted procedure of calculating the effects of varying α by simply reconverging selected models of the $\alpha = 1.0$ sequences, changing only the value of α assumed, will tend to overestimate the resultant change in $\log L$. This source of error, while small, should be kept in mind since the age of a *metal-rich* star cluster, if derived largely from a comparison of its subgiant branch with those of a relevant set of isochrones, will be too high by -6%. A final point should be made regarding the effects of the mixing-length parameter. Since the change in $\log T_{eff}$ produced by a change in α is considerably smaller in the neighborhood of the main sequence than it is at the red giant branch, a larger value of α will therefore be reflected in a steepening of the slope of the subgiant branch of a theoretical isochrone of a given age.

Thus far, little has been said about the consequences of employing our adopted opacities (see § II*b*) in preference to the oft-used Cox and Stewart (1970*a*, *b*) data. We have already noted that the former are generally higher than the latter at many temperatures and densities characteristic of stellar interiors, at least for metal-rich compositions (see Magee, Merts, and Heubner 1975), and Alexander (1975) has shown that the Cox-Stewart opacities are clearly deficient at low temperatures because of their neglect of important molecular sources. As a result, stellar models based on the improved opacity calculations would be expected to be cooler and less luminous than those obtained previously. This prediction is borne out, as we see, in Figure 4, which compares the location in the H-R diagram of our $\alpha = 1.0$ main-sequence loci for $Z = 10^{-2}$ and $Z = 10^{-4}$ with the corresponding ones computed on the assumption of the Cox-Stewart opacities by Mengel *et al.* (1979). The positions of the 0.9 and $1.1 M_{\odot}$ models have been

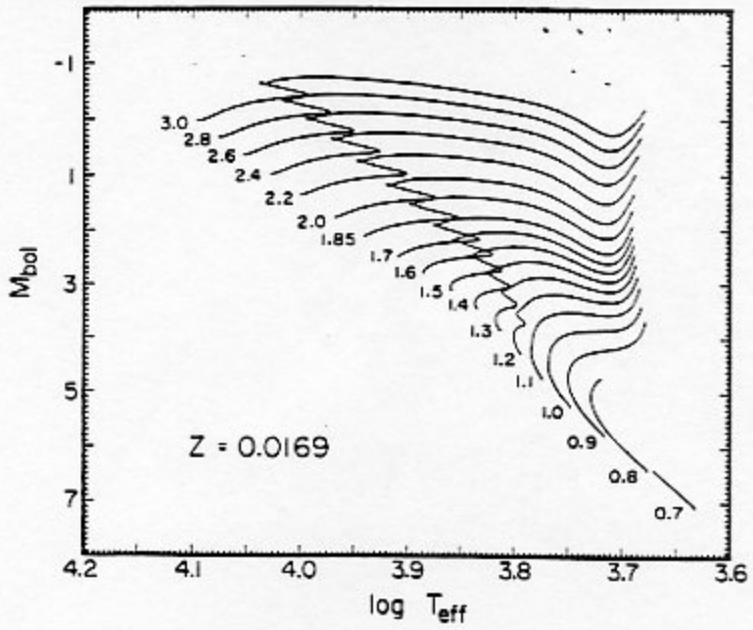

FIG. 1.—Evolutionary sequences for $Z = 0.0169$, assuming $Y = 0.25$ and $\alpha = 1.6$. Each track is labeled adjacent to the ZAMS location by its mass in solar units.

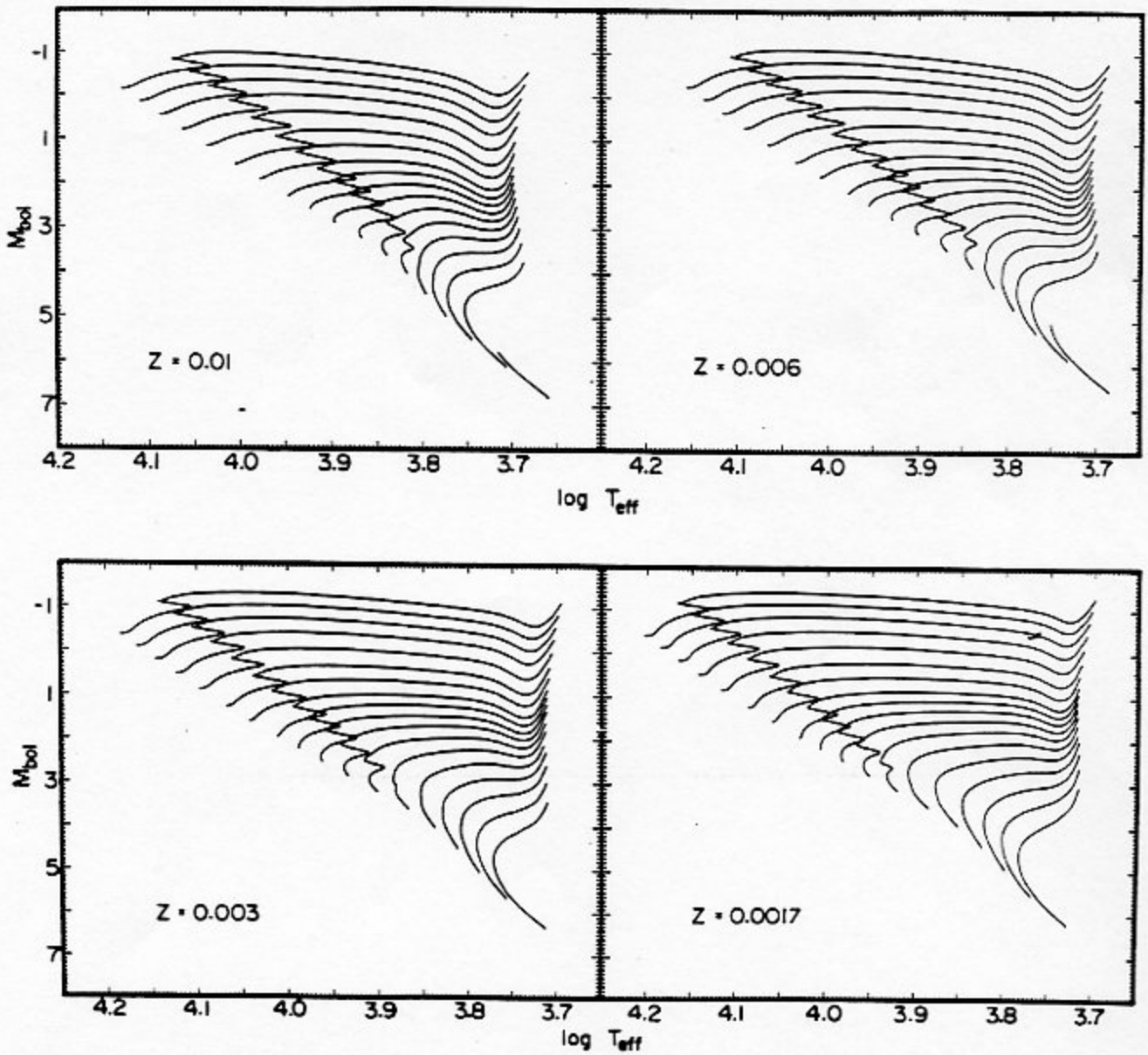

FIG. 2.—Evolutionary sequences for $0.01 \geq Z \geq 0.0017$, assuming $Y = 0.25$ and $\alpha = 1.6$. Each grid was computed for the identical run of stellar mass specified in Fig. 1.

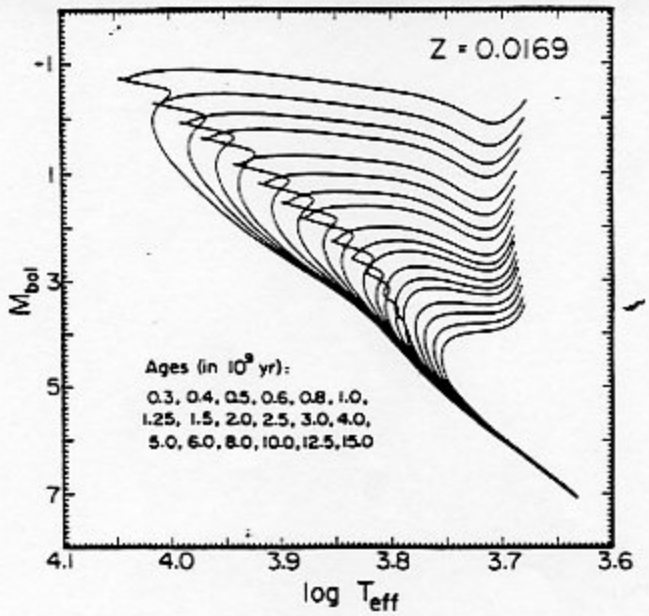

33

FIG. 4.—The isochrones which have been calculated from the evolutionary tracks illustrated in Fig. 1. The indicated ages apply to the isochrones in the order of decreasing turnoff luminosity.

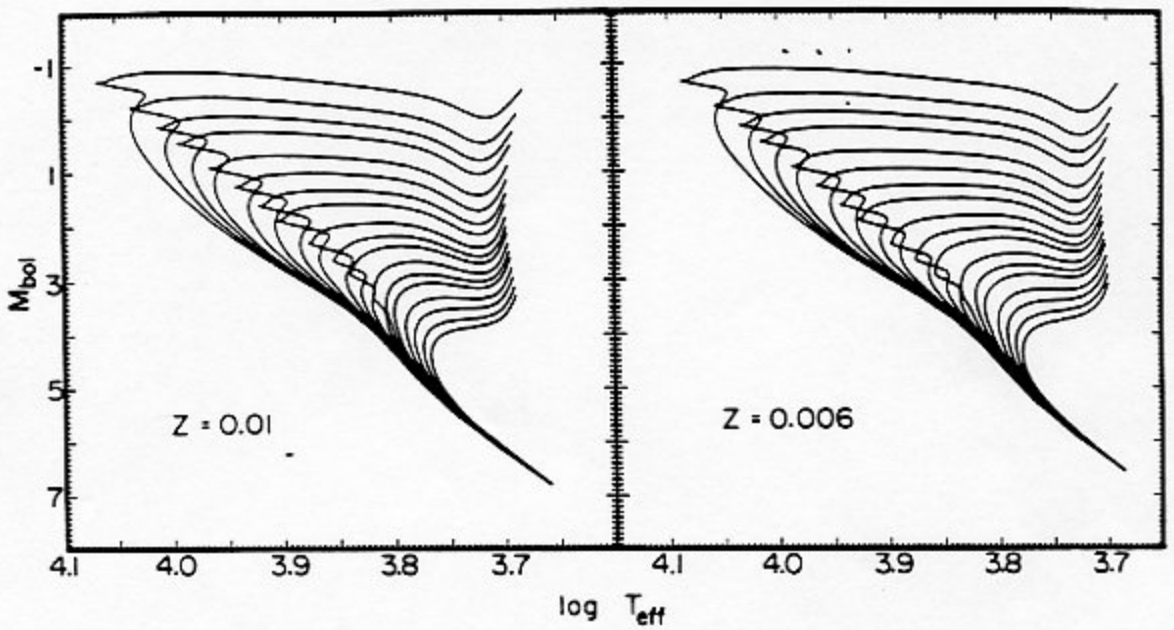

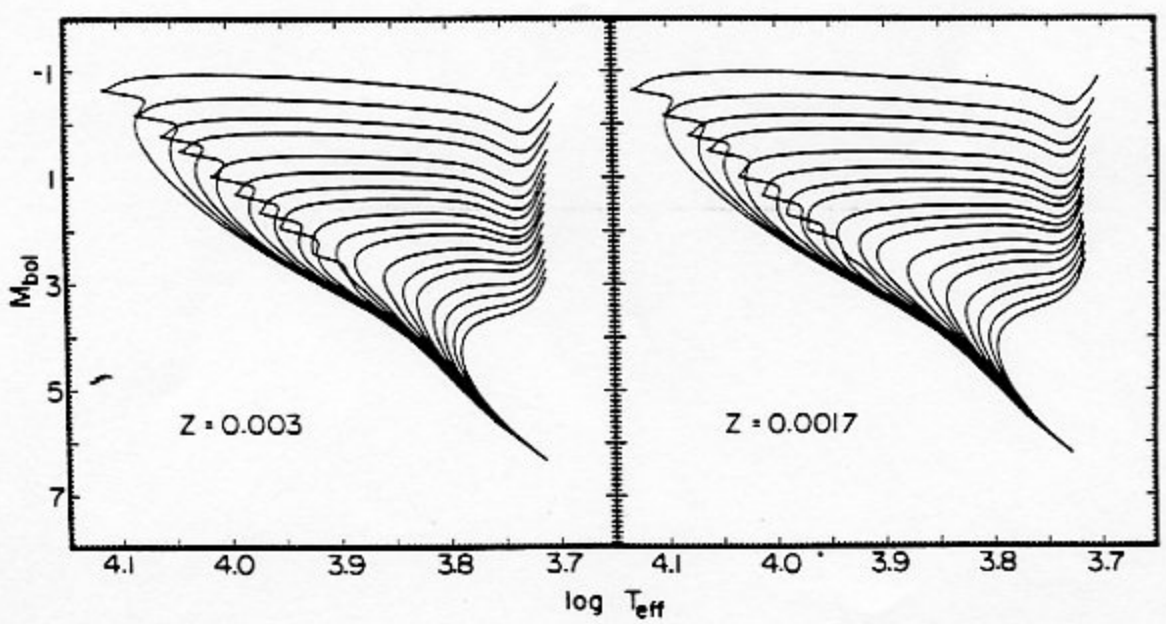

FIG. 5.—The isochrones which have been calculated from the evolutionary tracks illustrated in Fig. 2. These have been computed for the identical run of ages specified in Fig. 4.

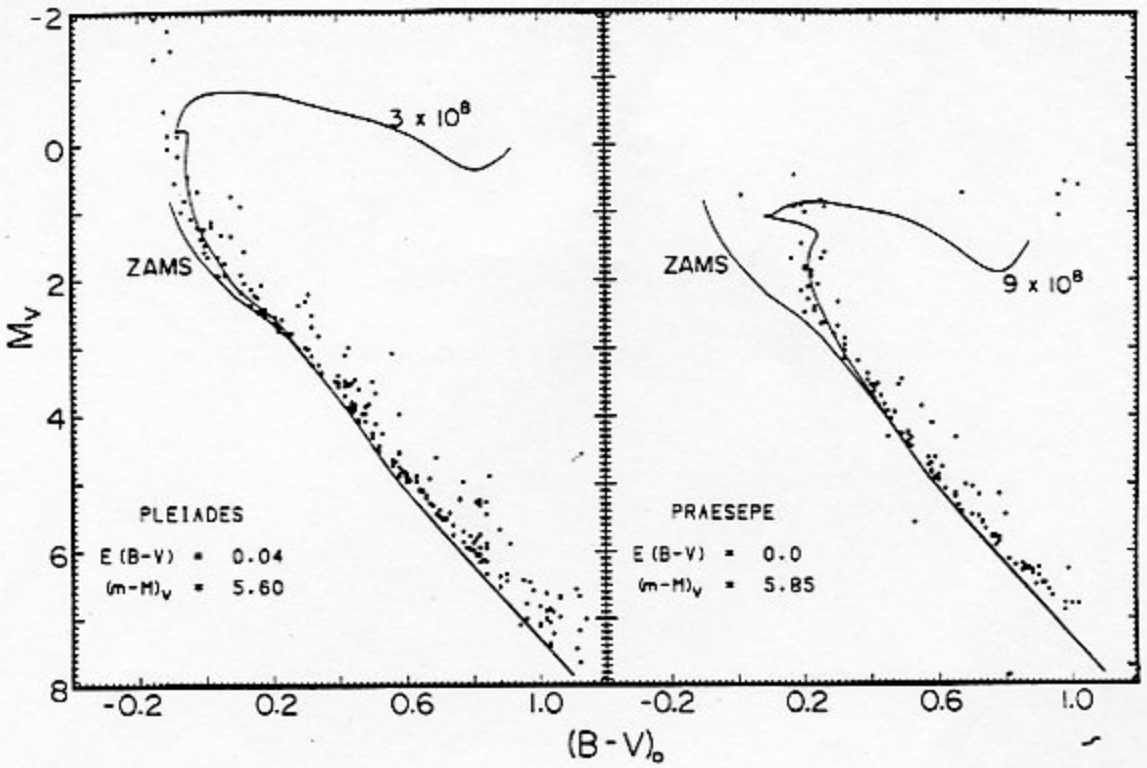

FIG. 7.—Comparison on the observational plane of selected isochrones (*solid curves*), as tabulated in this study, with published observations (*filled circles*) of the Pleiades and Praesepe star clusters. The sources of the photometry are given in Table 4. In each case, the cluster name and the adopted reddening and apparent distance modulus are specified in the lower left-hand corner. Isochrone ages in years are indicated near the base of the red-giant branch.

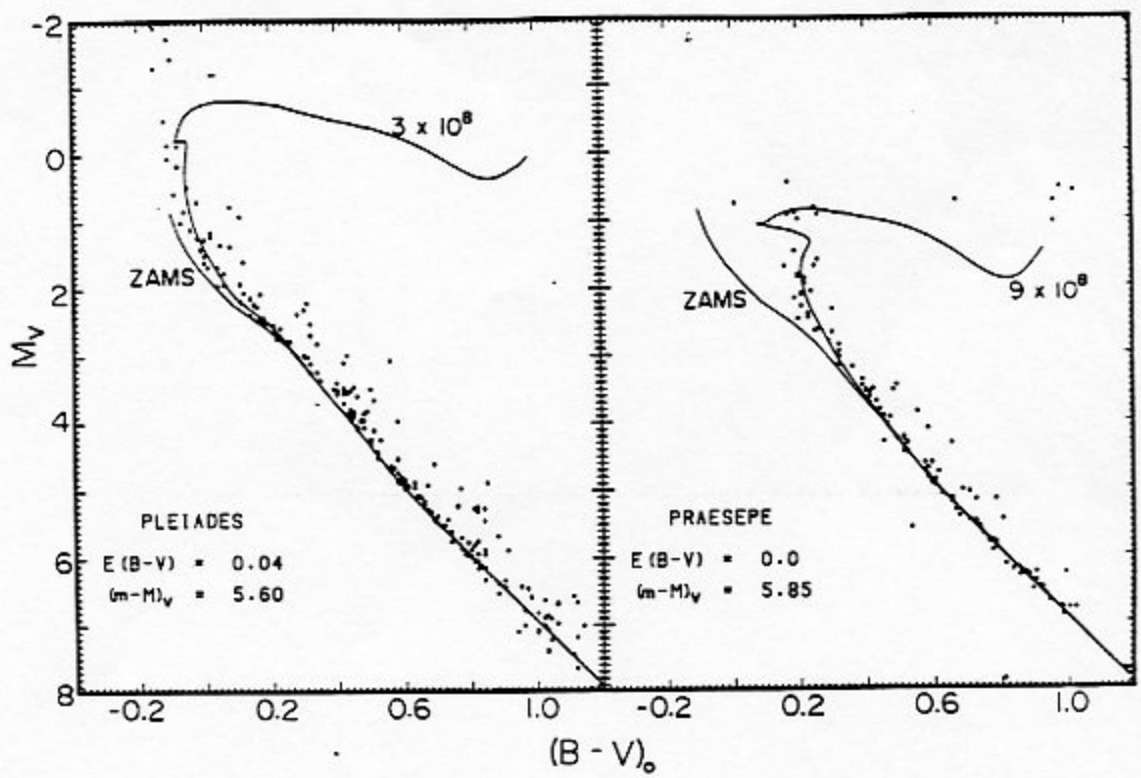

FIG. 8.—Similar to Fig. 7; in this case, the theoretical isochrones include the suggested empirical correction to the colors given by eq. (1).

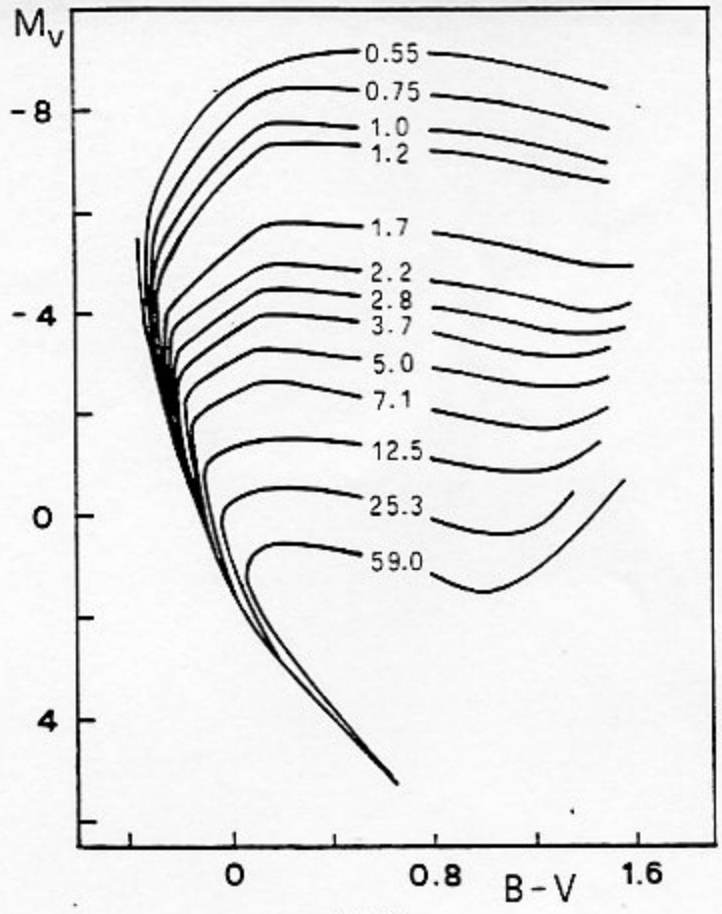

35

FIG. 23
Isochrones derived from the evolutionary star models of Fig. 22. Ages are given in units of 10^7 years (ref. 6).

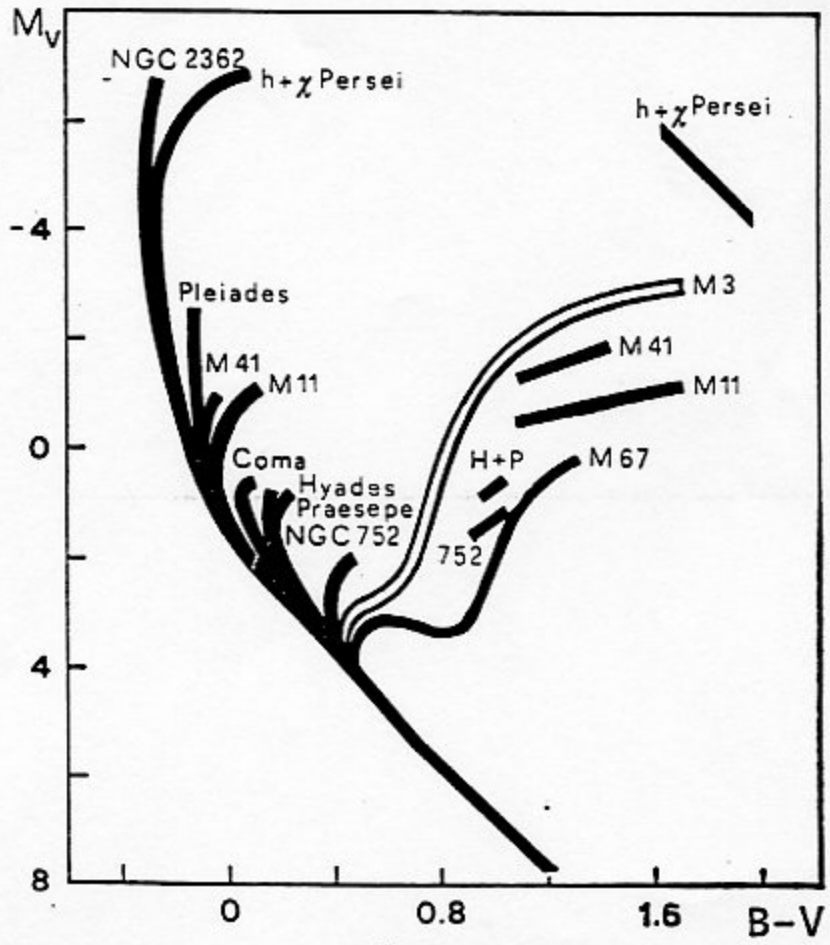

36

FIG. 21
Composite colour—magnitude diagram of ten open clusters and of one globular cluster (ref. 81).

M=1 Z=0.02 Stellar Evolution Tutorial

1. Core Hydrogen Burning (M = 1 Msun and Z=0.02)

1. We start by looking at the evolution of a star very similar to the Sun: it has the same mass and almost the same composition.

2. The figure below shows the HR diagram for the main H burning phases. The star starts on the zero-age main-sequence (ZAMS) and evolves off it and, following the exhaustion of the core H supply, it begins to ascend the giant branch. We will cover these in more detail below.

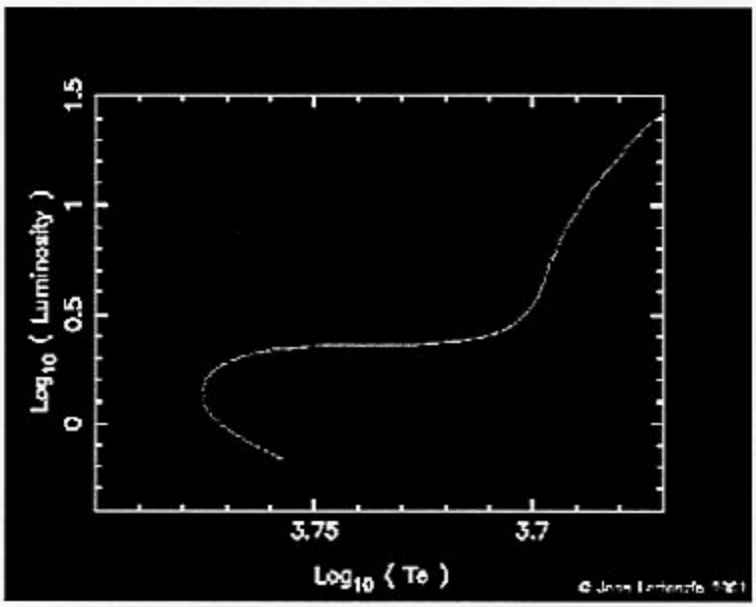

3. This movie (horizontal or vertical) shows the hydrogen profiles (ie H mass-fraction versus mass) in the centre of the star as it evolves off the main-sequence. This phase ends when the central H supply is exhausted. Note that each frame corresponds to one of the symbols in the HR diagram.

4. Of course, the burning of H proceeds more quickly in the very centre, where the temperature is higher. And it produces He (strictly, He-4) as the H is destroyed, as shown in this movie

5. Because we are using mass-fractions, then whatever H is burned will appear as He. This conservation of mass is nicely shown in the following movie which shows both H and He profiles during the H burning phase.

6. H burning in this star occurs via the PP chains, mostly, because it is not hot enough for substantial CN cycling. However, the CN cycle has reached equilibrium and we see the conversion of C-12 into N-14. As the star heats we see the advance outward of the region where CN reaches equilibrium. Toward the end of the main sequence the temperature becomes high enough for some ON cycling and we see the beginning of the conversion of

O-16 into N-14. This there are two steps in the N-14 profile: the first from the CN cycle converting C-12 into N-14. The second is from the ON cycle converting some O-16 into N-14.

7. The conversion of H into He raises the average mass per particle, usually measured by mu. For a perfect gas the pressure is given by

$$P = \rho R T/\mu$$

and since the pressure is constant (to first order) then as mu increases so must rho and T. That is, the centre of the star gets hotter and more dense, as shown in the following movies.
   1. Temperature
   2. Density

2. Shell Hydrogen Burning (M = 1 Msun and Z=0.02)

1. After the central H supply is all converted into He-4, we see the formation of a H-burning shell. This sits on the edge of the H-exhausted core and progresses outward (in mass! not in radius!) as the star evolves. The star now moves relatively rapidly away from the main sequence and toward the giant branch. This, and the advance of the H shell, is shown in the next movie (horizontal or vertical).

2. At the same time the CN profile hardly changes, as the top of the H shell has not moved very much. Rather, the H shell is advancing through the variable H profile left from the main-sequence evolution. But as the core contracts, the shell heats and we see the growth of the ON cycle, as reflected in the conversion of O-16 into N-14 in the next movie.

3. Once the H supply is gone in the centre then there is no nuclear energy generation. The luminosity is just the integral of the energy generation rate over mass, and there is no longer any nuclear energy generation (there is instead some gravitational energy liberation due to the core's contraction, but this is not very large compared to the previous nuclear source). And since the temperature gradient (in the diffusion approximation) is proportional to L, then the gradient is zero, and we have an isothermal core. At least, if there was no gravitational contraction it would be isothermal. So rather we have a nearly isothermal core. This is shown in the next two movies showing the formation of a core, its initial isothermal nature, and then we see the contraction cause it to increase somewhat in the centre. But there is a clear separation between the high density, nearly isothermal H-exhausted core, and the H-rich outer envelope. Note the very steep temperature and density gradient at the edge of the He-core.
   1. Temperature
   2. Density

3. First Dredge-Up (M=1 Msun, Z=0.02)

As the star ascends the giant branch it grows in radius and the outer envelope cools. Convection becomes the dominant energy transport mechanism due to the increased opacity at these lower temperatures. The innermost edge of the convective envelope moves inward as shown below.

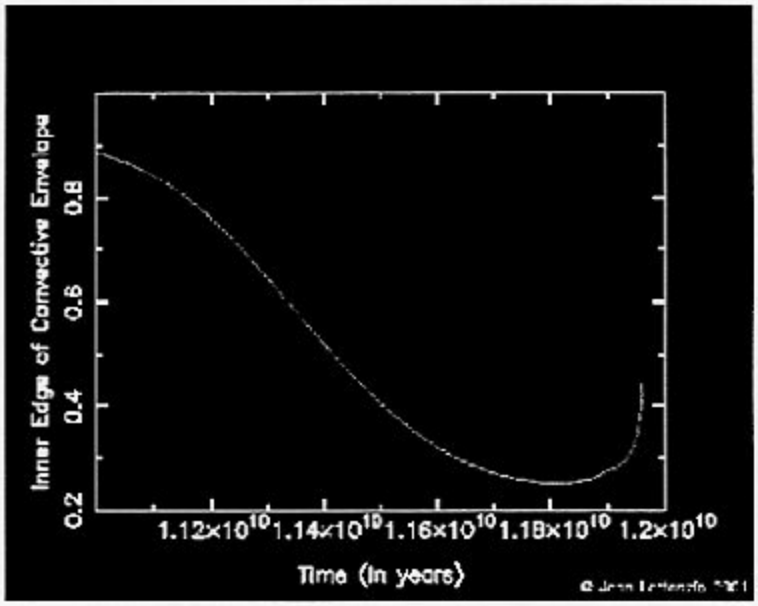

The next movie (horizontal or vertical) shows the corresponding position in the HR diagram.

1. As the convection extends inwards it can reach into regions where there was H burning during earlier phases. The figure below shows the H profile at a time during this phase. Convective regions are shown in red, and radiative regions in green. The convection thus reaches into the interior and "dredges-up" some products of earlier H burning. This is called the "First Dredge-up" phase.

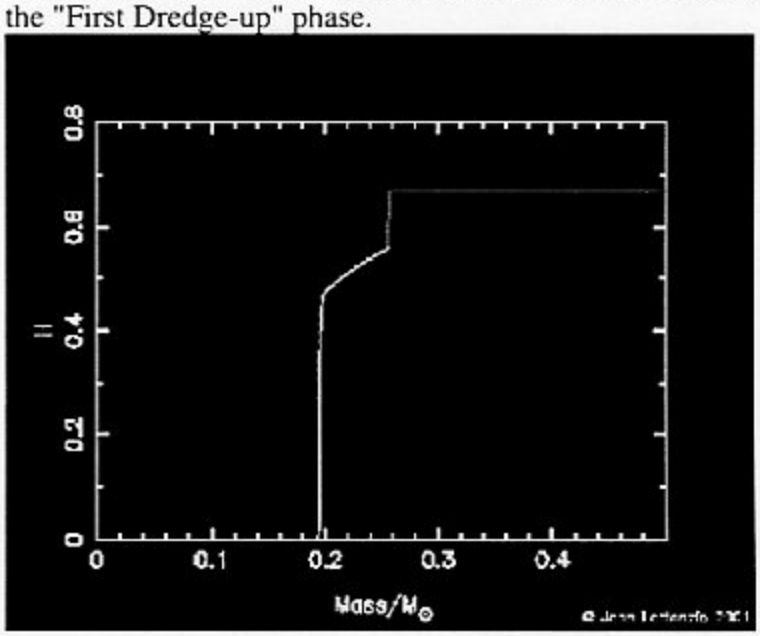

The next movie (horizontal or vertical) shows the H profiles and the corresponding position in the HR diagram.

2. Where the H has been burned to He there has been CN cycling producing N-14 from C-12. Hence the First Dredge-Up will be accompanied by the increase in the envelope abundance

of N-14 and a decrease in the C-12 content. This is shown in the next two movies:

1. C-12 profiles during First Dredge-Up (horizontal or vertical)
2. N-14 profiles during First Dredge-Up (horizontal or vertical). Note the second rise in N-14, due to the ON cycle operating further inward (where the temperature is higher).
3. C-12 profiles and inner edge of the convective envelope (horizontal or vertical)
4. C-12, N-14 and O-16 profiles during First Dredge-Up. This shows the growth inward of the convective envelope as well as the advance outward of the ON cycling part of the H-burning shell

4. The Bump in the Luminosity Function (M=1 Msun, Z=0.02)

1. When the convection retreats again it leaves behind a discontinuity in the abundance profiles. When the H shell reaches this point it suddenly finds the abundance to be larger than required for the current structure of the shell. A hydrostatic readjustment of the structure follows, and during this the luminosity actually decreases slightly, albeit briefly, before the star continues its ascent of the giant branch. This can be seen in the next movie (horizontal or vertical).

2. This (temporary) reversal of the direction of evolution means that there are more stars seen in this region of the HR diagram than just above or below. This causes a bump in the luminosity function of clusters.

5. Overview of H Burning (M=1 Msun, Z=0.02)

1. Now is a good time to review the overall evolution during the main H burning phases. The movies below will do this. There is a frame in each movie corresponding to each symbol in the HR diagram below.

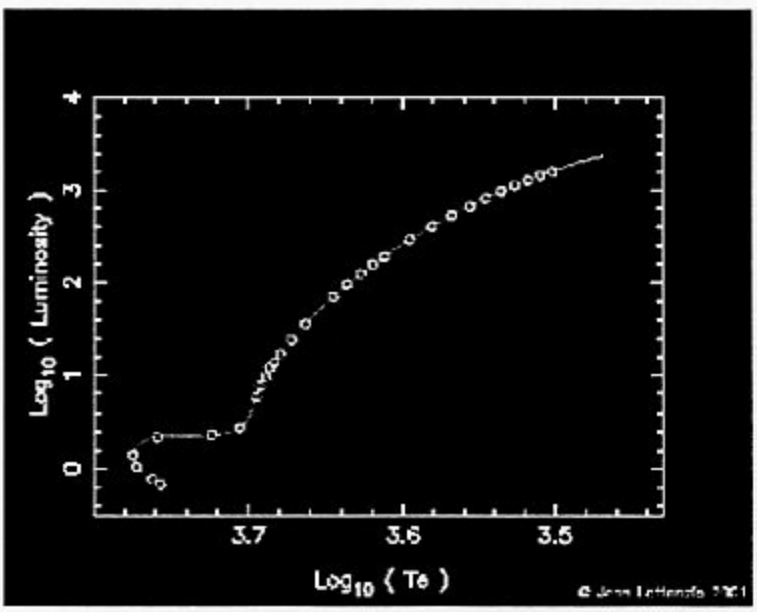

2. Firstly we show the dramatic increase in radius as the star ascends the giant branch in the following movie (horizontal or vertical).

3. As the star's radius swells, the material is less tightly bound gravitationally to the star. Also, the increased luminosity increases the linkage between grains in the envelope and the gas comprising the star. Hence the mass-loss rate increases. Here we used a Reimers mass-loss formula, and the resulting decrease in mass is shown here (horizontal or vertical).

4. The next movies colour coding to illustrate certain features of the star. Wherever all the H has been burned we draw the line in green. Where the H still has the surface value we draw the line in dark blue. In between, where the H abundance is somewhere between zero and the surface we draw the line in cyan. this indicates the position of the H-shell, or the regions of variable H abundance. An example of such a frame is shown below, where we plot temperature vs mass. You can see the isothermal H-exhausted core (in green) very clearly. The H shell is indicated in cyan, and this figure shows how narrow is the H-shell (in mass).

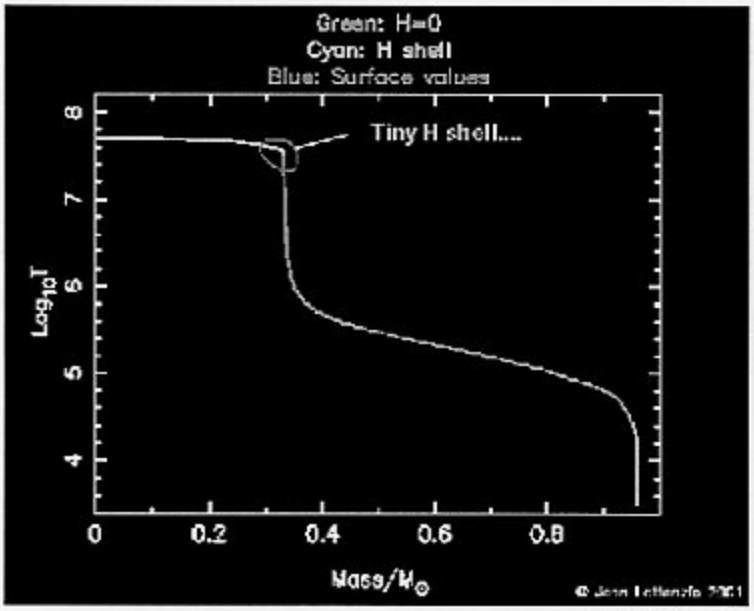

5. The next movie shows the H profiles along the HR evolutionary track (horizontal or vertical). Note that the outer edge of the graph moves inward, reflecting the decrease in the total mass of the star.

6. Here we show the temperature profiles during the H-burning evolution. Watch the formation of the isothermal core, once H is exhausted in the centre. Look also at how quickly the H shell thins to a tiny cyan dot!)

7. This movie shows the density profiles. Again, we clearly see the formation of the He-core and the very thin H-shell.

6. The Core Helium Flash (M=1 Msun, Z=0.02)

1. We resume the evolution as the star ascends the giant branch. The He core is contracting and gradually heating, but it is also getting denser and more degenerate. A completely degenerate gas has a polytropic equation of state, which means that the pressure is given by

$$P = K \rho^{\gamma}$$

II.3 Red Giants ~~and the Topology of the U-V Plane~~

First Dredge-Up

As a star ascends the giant branch, the cool temperature leads to increasing opacitiy, and the envelope becomes convective. Indeed, the star is moving along the edge of the Hayashi forbidden zone, so that convection extends over as much of the star as is possible. This means that it extends virtually all the wayt down to the hydrogen-burning shell. In most cases, this means that the convection has reached into regions where there has been some burning of hydrogen earlier in the stars life. For example, the outer edge of the receding convective core, for more massive stars, or the outer parts of earlier central H burning for less massive stars. Thus the products of this H burning are then mixed to the surface of the star by the convection. This is called "dredge-up". The material which is brought to the surface has been exposed to H burning, so H has been converted into He, and C has been converted into N via the CN cycle (it is not hot enough for the ON cycle to operate).

see Fig A
see Notes x1

Homology Invariants

When considering stars of different masses M and M' and radi R and R' we define "homologous" points to be those where $r/R = r'/R'$. We then say two stars are homologous if their homologous mass shells $m/M = m'/M'$ are located at homologous points. Since these stars also satisfy the stellar strcuture equations, then this homology requirement has repercussions for other variables. We will not deal with this in detail, but we note that a variable which remains unchanged in homologous stars is called a "homology invariant". Two important homology invariants for polytropic stars are

$$U = \frac{d\ln m}{d\ln r} \qquad V = -\frac{d\ln P}{d\ln r}.$$

Here we take $P = K\rho^\gamma$ and $\gamma = 1+1/n$, where n is the polytropic index. Now, this is the usual choice, but Peter Eggleton (from the Institute of Astronomy, Cambridge) prefers the following invariants:

$$U' = -\frac{d\ln m}{d\ln P} \qquad V' = -\frac{d\ln r}{d\ln P}.$$

Further, we will write

$$\rho = P^s$$

which has the advantage that as γ decreases through unity (isothermal) s is well behaved whereas n passes through ∞ and then becomes negative. Also, we note that for a finite mass we want $\frac{d\ln m}{d\ln p} \to 0$ at the surface (or else the mass continues to increase). Likewise, for a finite radius we want $\frac{d\ln r}{d\ln p} \to 0$. Note that these simple correspond to $U' = V' = 0$. Clearly, we also have

$$V' = -\frac{1}{V} \qquad U' = \frac{U}{V}.$$

Exercise: Check that U, V, U' and V' are homology invariants.

If a star is in hydrostatic equilibrium then we must have

$$\frac{dm}{dr} = 4\pi r^2\rho$$
$$\frac{dP}{dr} = -\frac{\rho Gm}{r^2}.$$

If we use these, then we can show that

$$U = \frac{4\pi r^3\rho}{m} \qquad U' = \frac{4\pi r^4 P}{Gm^2}$$
$$V = \frac{Gm\rho}{rP} \qquad V' = \frac{rP}{Gm\rho}$$

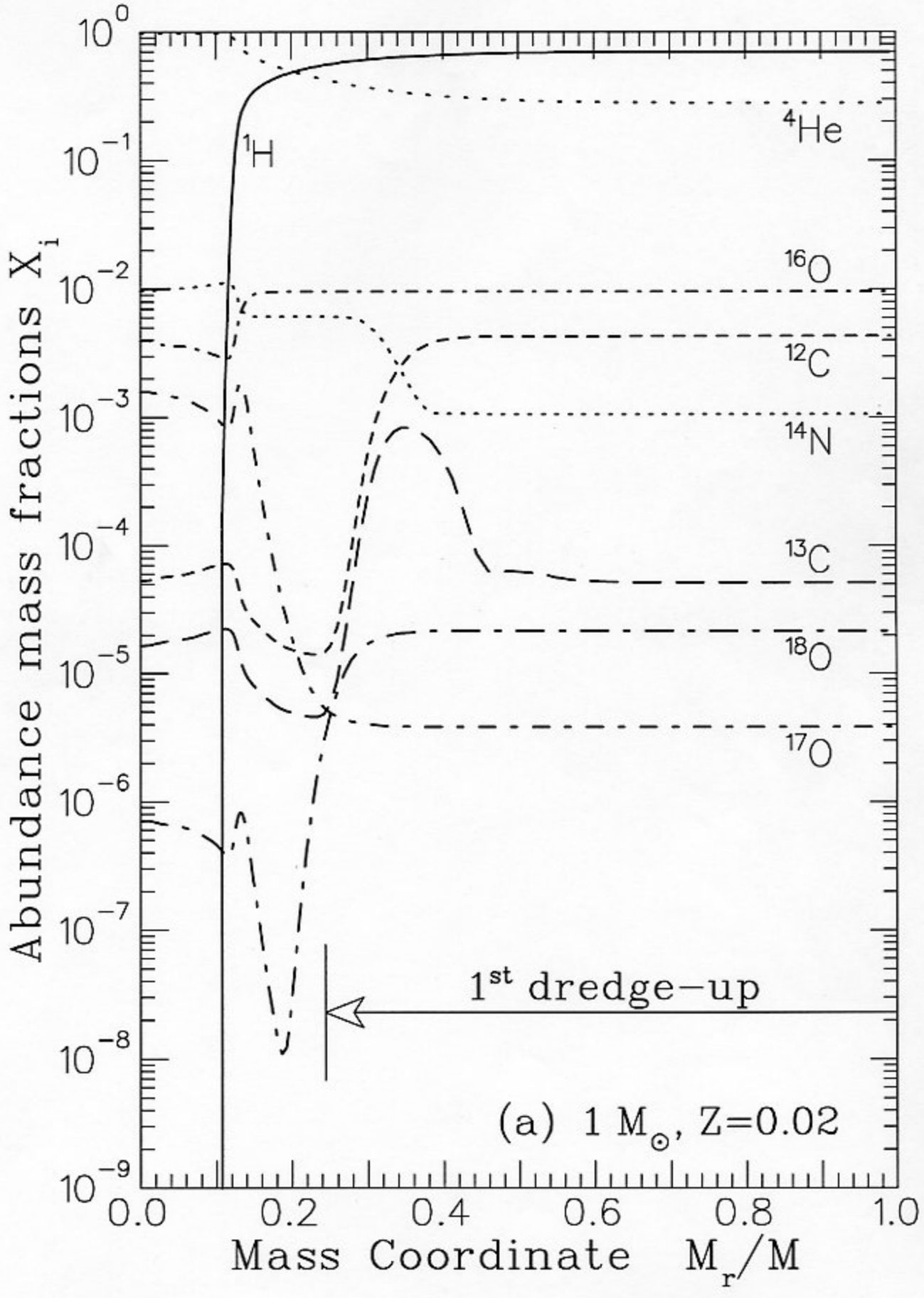
Abundance mass fractions X_i
10^0
10^{-1}
10^{-2}
10^{-3}
10^{-4}
10^{-5}
10^{-6}
10^{-7}
10^{-8}
10^{-9}
^{1}H
^{4}He
^{16}O
^{12}C
^{14}N
^{13}C
^{18}O
^{17}O
1st dredge-up
(a) 1 $M_\odot$, Z=0.02
0.0
0.2
0.4
0.6
0.8
1.0
Mass Coordinate M_r/M

Fig A

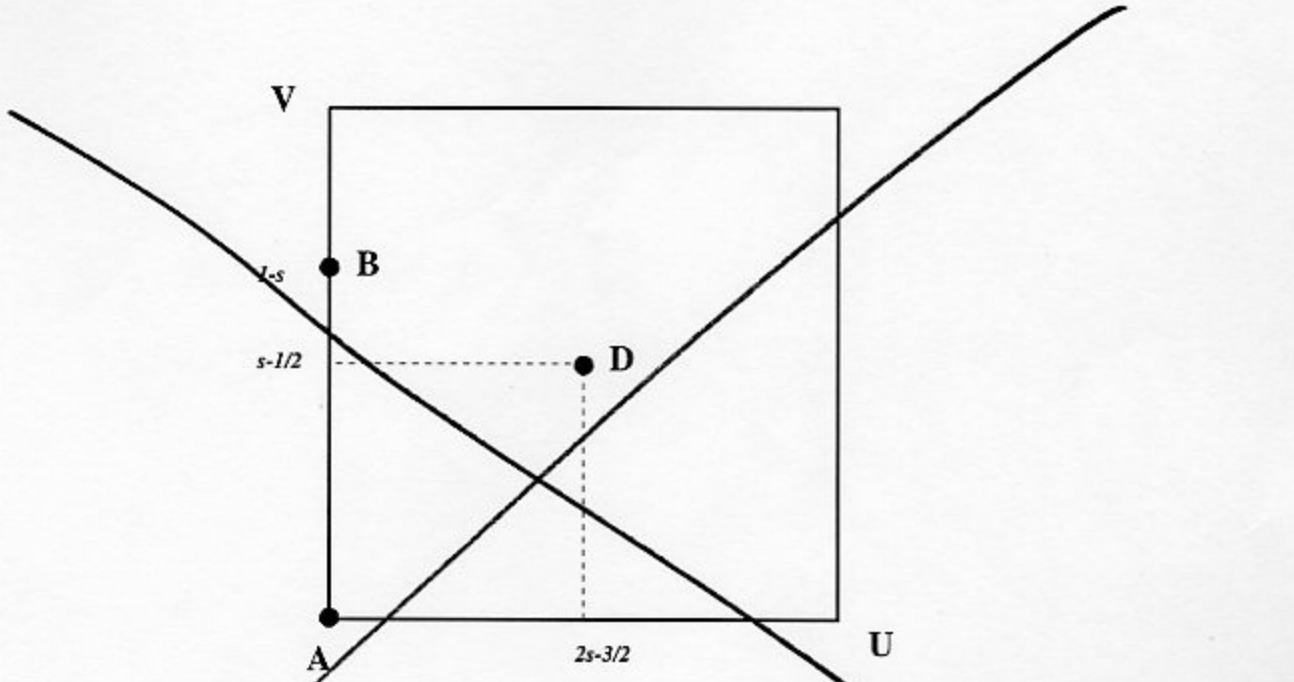

Sketch of Critical Points in the U–V plane.

The summary situation is shown in the figure below. We can summarise by looking at the various cases.

$s < 3/4$ Here we have a stable node at A, and an unstable node at B. All configurations have finite mass and radius, as all phase paths end at the origin.

$3/4 < s < 5/6$ Point A remains stable, and point D enters. One path links D to B, and B is unstable. All others end at the origin, which has finte mass and radius. When s reaches $s^\star$ then point D changes from a node to a spiral.

$5/6 < s < 1$ D becomes stable. A path from infinity ends at B. Lower paths end at A and are finite. Those above D ar enot.

~~$1 < s$ B leaves the plane, A is unstable, and all solutions go to D, with a non-zero U~~ and V. Thus M and R are no longer finite.

Thus we conclude that for a red-giant to form we require $s > 5/6$ (or $n > 5$ somewhere. Not necessarily throughout the structure, but somewhere.

An alternative way of looking at the situation, is the following. We have a core, which is contracting slightly. Outside this is a nuclear burning shell. This is shown in the figure below. The nuclear shell keeps the temperature roughly constant. But by simple scaling of the differential equation, we see that to order of magnitude $T \sim 1/r$. Thus we can think of the nuclear burning shell as keeping the radius of the core roughly constant. But without nuclear burning in the core, gravitational contraction causes some contraction. So the core's central density rises. As the advancement of the shell is only slowly adding mass to the core, we can take this mass to be constant. Then as the density in the centre rises, then density at the edge of the core must decrease. Now, the mass outside the core is also constant. Yet the density at the bottom of the envelope is decreasing. This to encompass the whole mass the radius must extend. Hence the radius grows.

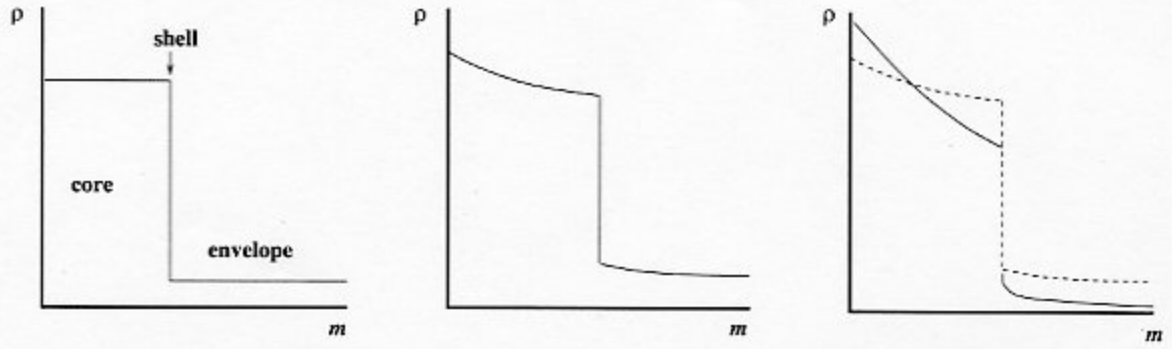

Schematic evolution of core and envelope in a Red-Giant.